



Published in final edited form as:

Cell Tissue Res. 2022 May ; 388(2): 373–398. doi:10.1007/s00441-022-03602-3.

Transcriptomic and Ultrastructural Evidence Indicate That Anti-HMGB1 Antibodies Rescue Organic Dust Induced Mitochondrial Dysfunction

Sanjana Mahadev Bhat^{1,2,§}, Nyzil Massey¹, Denusha Shrestha¹, Locke A. Karriker³, Tomislav Jelesijevi⁴, Chong Wang^{3,5}, Chandrashekhar Charavaryamath^{1,*}

¹Department of Biomedical Sciences, Iowa State University, Ames, IA, USA.

²Immunobiology Interdepartmental Graduate Program, Iowa State University, Ames, IA, USA.

³Department of Veterinary Diagnostic and Production Animal Medicine, Iowa State University, Ames, IA, USA.

⁴Department of Comparative Biological Sciences, Louisiana State University, Baton Rouge, LA, USA.

⁵Department of Statistics, Iowa State University, Ames, IA, USA.

§ Current affiliation: Department of Physiology and Biomedical Engineering, Mayo Clinic, Rochester, MN

Abstract

Exposure to organic dust (OD) in agriculture is known to cause respiratory symptoms including loss of lung function. OD exposure activates multiple signaling pathways since it contains a variety of microbial products and particulate matter. Previously, we have shown how OD exposure leads to the secretion of HMGB1 and HMGB1-RAGE signaling, and how this can be a possible therapeutic target to reduce inflammation. Cellular mitochondria are indispensable for homeostasis and are emerging targets to curtail inflammation. Recently, we have also observed that OD exposure induces mitochondrial dysfunction characterized by loss of structural integrity and deficits in bioenergetics. However, the role of HMGB1 in OD-induced mitochondrial dysfunction in human bronchial epithelial (NHBE) cells remains elusive. Therefore, we aimed to study whether decreased levels of intracellular HMGB1 or antibody-mediated neutralization of secreted

*To whom correspondence should be addressed: Chandrashekhar Charavaryamath, BVSc, MVSc, PhD., Assistant Professor, Department of Biomedical Sciences, Iowa State University, Ames, IA 50011. Telephone: (515) 294-7710; Fax: (515) 294-2315; chandru@iastate.edu.

Author Contributions

S.M. Bhat participated in the design of experiments, performed the experiments, analyzed the data, and wrote the manuscript. N. Massey performed organic dust extraction. D. Shrestha assisted in culturing of NHBE cells. L. Karriker collected the organic dust samples and edited the manuscript. T. Jelesijevi provided the technical expertise required to perform fluorescent microscopy and participated in editing the manuscript. C. Charavaryamath conceptualized the study, participated in the design of the experiments, performed dust extraction, participated in the interpretation of data, and edited the manuscript. All authors have read and approved the final manuscript.

Conflict of Interest

The terms of this arrangement have been reviewed and approved by Iowa State University per its conflict-of-interest policies. All other authors have declared no potential conflicts of interest. The authors declare that the research was conducted in the absence of any commercial or financial relationships that could be construed as a potential conflict of interest.

HMGB1 would rescue mitochondrial dysfunction. Single and repeated ODE exposure showed an elongated mitochondrial network and cristolysis whereas HMGB1 neutralization or the lack thereof promotes mitochondrial biogenesis evidenced by increased mitochondrial fragmentation, increased Drp1 expression, decreased Mfn2 expression, and increased PGC1 α expression. Repeated 5-day ODE exposure significantly downregulated transcripts encoding mitochondrial respiration and metabolism (ATP synthase, NADUF, and UQCR) as well as glucose uptake. This was reversed by the antibody-mediated neutralization of HMGB1. Our results support our hypothesis that in NHBE cells neutralization of ODE-induced HMGB1 secretion rescues OD-induced mitochondrial dysfunction.

Keywords

Organic Dust; HMGB1; Airway Inflammation; Mitochondrial Dysfunction; Mitochondrial DNA

INTRODUCTION

An increase in human population has led to an increased demand for protein through meat. Hence, animal production system has transformed into a large-scale concentrated animal feeding operations (CAFOs). These CAFOs generate many on-site contaminants that pose a threat to workers, animals, and the environment. Agriculture workers who are exposed to the airborne contaminants are at an increased risk of developing respiratory and other symptoms (Nordgren and Charavaryamath 2018). The on-site contaminants in CAFOs mainly include airborne organic a (OD), gases, and other microbial components.

The OD is a complex mixture of various microbial associated molecular patterns (MAMPs) including endotoxin, peptidoglycans, Gram-positive bacterial components, (1 \rightarrow 3)- β -D-glucans, and fungi which are all important pro-inflammatory inflammagens (Poole and Romberger 2012; Nordgren and Charavaryamath 2018; Poole et al. 2019; Kelly and Poole 2019). Repeated exposure of workers to this complex OD has been associated with respiratory disease development and severity. Exposed workers report a variety of respiratory symptoms and suffer from asthma, chronic bronchitis, and chronic obstructive pulmonary disease (COPD) (Charavaryamath and Singh 2006; May et al. 2012; Poole and Romberger 2012; Wunschel and Poole 2016; Warren et al. 2019). Due to the complex nature of the OD, several research studies have targeted various pattern recognition receptors (PRRs) and the respective downstream regulators as a strategy to reduce the severity of OD-induced airway diseases. For example, a few groups have targeted various PRRs and signaling molecules including TLR2, TLR4, NOD2, protein kinase C, and MyD88 (Poole et al. 2007, 2010, 2011; Charavaryamath et al. 2008; Bailey et al. 2008; An et al. 2020). Recently, we examined various kinome (set of protein kinases) signaling pathways in human airway epithelial and monocytic cell lines following OD exposure and concluded that exposure induces several overlapping innate inflammatory signaling pathways indicating a complex host response (Nath Neerukonda et al. 2018).

Airway epithelial cells are central to the first line of defense against the danger signals encountered in the lungs (Whitsett and Alenghat 2015). Exposure of lung epithelial cells

to OD has been shown to trigger oxidative stress, cytokine release, cellular dysfunction, and eventually cell death which are key processes involved in the pathogenesis of airway inflammation (Charavaryamath and Singh 2006; Poole and Romberger 2012; Sethi et al. 2017; Bhat et al. 2019). Mitochondria (mt) are indispensable organelles and are referred to as the powerhouse of the cells. Emerging data have identified a pivotal role of mitochondria in several inflammatory airway diseases (Prakash et al. 2017). Therefore, mitochondria represent an attractive therapeutic target in rescuing airway epithelial cells from the negative effects of chronic exposure to OD.

Alterations in mitochondrial morphology and function have been documented in airway epithelial cells in cases of COPD and asthma (Schumacker et al. 2014; Cloonan and Choi 2016; Piantadosi and Suliman 2017; Prakash et al. 2017; Fetterman et al. 2017; Aghapour et al. 2019). This includes a decrease in oxidative phosphorylation (OXPHOS) and Krebs cycle enzymes, blunted mitochondrial respiration, and suppressed respiratory reserve, resulting in enhanced reactive oxygen species generation (ROS), which can, in turn, modulate mitochondrial morphology and function orchestrating a vicious cycle of inflammation and exacerbate airway disease. In addition to mitochondrial dysfunction, mitochondrial damage and release of mitochondrial components either into the cytosol or extracellularly has been an emerging factor in the induction of inflammation (Cloonan and Choi 2012, 2016; Eisner et al. 2018; Aghapour et al. 2019; Cloonan et al. 2020). Mitochondrial damage-associated molecular patterns (mtDAMPs) perform as signaling molecules and activate PRRs such as TLRs and induce a myriad of inflammatory cascades (Rubartelli and Lotze 2007; Zhang et al. 2010; Cloonan and Choi 2012). In our recent study, we showed increased mitochondrial fusion and mitophagy, along with the leakage of mtDAMPs such as mitochondrial DNA (mtDNA) and mitochondrial transcription factor A (TFAM) upon exposure of THP1 cells to OD extract (ODE) (Mahadev Bhat et al. 2021). Recent studies have shown that the release of TFAM along with mtDNA amplifies the release of TNF α and type 1 interferon, thus promoting a sterile inflammation via the cGAS-STING pathway (Cantaert et al. 2010; CHAUNG et al. 2012; Julian et al. 2013). Collectively, understanding the mechanism of how mitochondria promote inflammation can help in developing effective mitochondria-targeted therapies to curtail OD exposure-induced airway inflammation. To develop such therapies, an understanding of the interactions between the host airway epithelial cells and its mitochondria during OD-induced inflammation is key.

High mobility group box 1 (HMGB1) is known to be a key player in the induction of sterile inflammation and a possible therapeutic target (Andersson and Tracey 2011). HMGB1 is an endogenous nucleoprotein, evolutionarily conserved, ubiquitously present and maintains nuclear homeostasis. This protein is secreted into the extracellular environment and acts as a prototypic DAMP and is important for oxidative stress response (Yang et al. 2015; Ugrinova and Pasheva 2017). Extracellular HMGB1 is a delayed mediator of inflammation when compared to other pro-inflammatory mediators and is shown to stimulate the release of multiple pro-inflammatory cytokines including tumor necrosis factor (TNF), interleukin (IL)-1, IL-6, IL-8, and macrophage inflammatory protein (MIP)-1 (Yang et al. 2015; Bhat et al. 2019; Massey et al. 2019, p. 1). The use of neutralizing monoclonal anti-HMGB1 antibodies *in vivo* has been shown to ameliorate tissue injury and reduce lethality (Zhou et al. 2009; Bhat et al. 2019).

Contemporary publications have demonstrated that siRNA-mediated knockdown of HMGB1 in macrophages and dendritic cells suppressed the release of HMGB1 and reduced the cytokine storm (Qin et al. 2006; Ye et al. 2012). We have previously shown the pro-inflammatory effects of extracellularly secreted HMGB1 on bronchial epithelial cells on exposure to ODE and how its neutralization abrogates ODE-induced inflammation (Nath Neerukonda et al. 2018; Bhat et al. 2019; Massey et al. 2019). Qi et al., directly correlated the alterations in mitochondrial function to the loss of HMGB1 and further demonstrated a significant decrease in basal OXPHOS and glycolysis along with decreased ATP output (Qi et al. 2015). Also, a lack of HMGB1 has been shown to promote mitochondrial fragmentation and loss of mitochondrial membrane potential (Tang et al. 2011). Therefore, we have raised pertinent questions as to what impact HMGB1 would have on mitochondrial morphology and function in bronchial epithelial cells on exposure to ODE.

In the current manuscript, we tested a hypothesis that, ODE-exposure of primary normal human bronchial epithelial (NHBE) cells induces mt-damage, dysfunction and targeting HMGB1 is protective. This study examined the impact of HMGB1 on mitochondrial biogenesis and function on ODE exposure by using NHBE cells. We tested this hypothesis by using a single (acute) and repeated (chronic) ODE exposure model with siRNA-mediated knockdown of HMGB1 and by neutralization of secreted HMGB1, respectively. Here we demonstrated that ODE exposure promotes the release of mtDAMPs and activation of cGAS-STING mediated signaling while knockdown of HMGB1 promotes mitochondrial biogenesis on single exposure to ODE. In the repeated exposure model, neutralization of extracellular HMGB1 is protective and maintains mitochondrial morphology, as well as upregulate pathways involved in mitochondrial respiration and biogenesis. Using an air-liquid interface (ALI) model, we show that neutralization of extracellular HMGB1 rescues ODE exposure-induced damages to epithelial integrity via its effect on tight junction proteins.

MATERIALS AND METHODS

Chemicals and reagents

We purchased NHBE – growth medium (Pneumacult-Ex media; BEGM) and differentiation media (Pneumacult-ALI media) from StemCell Technologies. MTT, CM-H₂DCFDA, 2-NBDG, MitoTracker green, and MitoSox Red dyes were purchased from Invitrogen (ThermoFisher Scientific) and Rhod-2AM dye was obtained from Abcam. Griess' reagent was purchased from Sigma-Aldrich. Antibodies used and their details have been listed in the Supplementary tables 4 and 5 respectively. Primers used and their sequences are listed in Supplementary table 2 and were synthesized at the Iowa State University's DNA facilities. TaqMan® Gene Expression Assay was purchased from Invitrogen (ThermoFisher Scientific). HMGB1 siRNA kit was purchased from Integrated DNA Technologies (IDT) and Anti-HMGB1 neutralizing antibody sample (Batch # Q2g7–47C, stock concentration 1.8 mg/mL) was a generous gift from Dr. Kevin Tracey's laboratory (Feinstein Institutes for Medical Research, Northwell Health, NY).

Organic dust extract preparation

Organic dust (OD) was collected and an aqueous extract was prepared as previously described (Romberger et al. 2002; Bhat et al. 2019). Settled surface dust samples from swine housing facilities were collected and 1 g of the dust was placed into sterile Hank's Balanced Salt Solution (10 mL; Gibco). The solution was incubated for one hour at room temperature, centrifuged for 20 min at 1365 x g to remove the larger coarse particles and microbes. The final supernatant was filter-sterilized (0.22 µm), a process that also removes coarse particles. Stock (100%) ODE aliquots were frozen at -20°C until use in experiments. The filter-sterilized organic dust extract (ODE) samples were considered 100% and diluted to 1–5% (v/v) before use in our experiments.

Endotoxin estimation

The concentration of endotoxin in the ODE samples were measured using the Pyrochrome[®] chromogenic endotoxin assay kit (Associates of Cape Cod, Inc., East Falmouth, MA). First, the samples were diluted in a ratio of 1:10 in endotoxin-free water. The samples along with reconstituted pyrochrome lysate were added to an endotoxin-free 96-well plate in a sample to lysate ratio of 1:4. Based on the manufacturer's recommendation, the standard was reconstituted and added to the plate in a sample to lysate ratio of 1:4. The microplate was incubated at 37°C with shaking and the absorbance was read at 405 nm (every 10 minutes, three readings over a total of 30 minutes) using the Gen 5[™] software in the BioTek[®] ELx808[™] spectrophotometer.

Cell culture and treatments

The de-identified human primary airway epithelial cells were obtained from the Mayo Clinic, Rochester, MN. These cells were collected at the Mayo Clinic under an approved Institutional Review Board (IRB) protocol. The lung tissues from patients undergoing thoracic surgeries for focal, non-infectious causes were collected. A trained pathologist identified the normal lung areas and airway epithelial cells were isolated from the third to sixth generation human bronchi. Iowa State University's Institutional Review Board considered these de-identified cells as exempt from approval. De-identified NHBE cells were also received through Dr. Kristina L. Bailey (University of Nebraska Medical Center, Omaha, NE). The NHBE cells were isolated from the human donors through the Live on Nebraska, an organ and tissue donation program. All the donors were deceased and an informed consent from the relatives was obtained by the Live on Nebraska. These de-identified NHBE cells were exempt from the Iowa State University's Institutional Review Board (IRB) approval. All the work was performed under an approved protocol from the Iowa State University's Institutional Biosafety Committee (IBC) approved protocol (IBC 19–004).

NHBE cells were seeded onto type-I bovine collagen (30 µg/mL; StemCell Technologies) coated T-75 flasks. Cells were grown submerged in BEGM (Pneumacult-EX) supplemented with 50X growth supplement (StemCell Technologies), 100 IU/mL penicillin, 100 µg/mL streptomycin (Gibco) and 1 µg/mL of Amphotericin B (Sigma-Aldrich). The cells were incubated in a humidified chamber with 5% CO₂ at 37°C until approximately around 60–70% confluence was achieved. All groups with treatment details are outlined in Figure 1.

The stock and working concentrations of the treatments are outlined in Table 2. Our *in vitro* models of single and repeated (five days) ODE exposure and treatments are represented in Figure 1a and 1b respectively. Cells were treated with either medium (control) or ODE (1% v/v) after HMGB1-specific siRNA mediated knock-down or co-treatment with anti-HMGB1 antibody for 24 hours (acute exposure) or 8 hours a day for 5 days (chronic exposure), respectively, with corresponding time-matched controls. Following treatments, samples were processed for various assays.

Air-Liquid Interface culture and treatment

Following subculture, NHBE cells were seeded onto 10.5 mm trans-well inserts (polyester membrane inserts with 0.4 μm sized pores; Corning) coated with type-I bovine collagen (30 $\mu\text{g}/\text{mL}$; StemCell Technologies, Vancouver, Canada) in 12-well plates. Cells were seeded at a density of $\sim 5 \times 10^3/\text{mm}^2$ in Pneumacult-EX expansion media (StemCell Technologies) onto the apical side of the insert, with the media in the basal chamber as well. The cells were maintained in the submerged culture conditions for 2–3 days incubated in a humidified chamber with 5% CO_2 at 37°C until a confluent monolayer was developed. Fresh medium (0.5 mL in the apical chamber and 1.0 mL in the basal chamber) was added every 48 hours to replace the spent media. Following attaining about 80% confluence, the expansion media in the apical and basal side was carefully removed and an ALI was developed by addition of the Pneumacult-ALI differentiation media (StemCell Technologies) in the basal chamber alone and incubated in a humidified chamber with 5% CO_2 at 37°C. Post airlift the cells were maintained for not more than 20 days. Fresh medium (1.0 mL in the basal chamber) was replenished every 48 hours and the apical surface of the monolayer was washed with DPBS twice every 48 hours to prevent mucus build-up.

Post differentiation, the apical surface of the cells was treated with either medium (control) or ODE (1% v/v) followed by a co-treatment with either Anti-HMGB1 neutralization antibody (10 $\mu\text{g}/\text{mL}$) or isotype-matched IgG controls (corresponding time-matched control) for 1 hour per day for 5 days. Following the treatments, samples were processed after 5 days for various assays. The exposure and treatments are outlined in Figure 1a.

siRNA mediated knockdown of HMGB1

Three (R1, R2 and R3) custom designed double-stranded anti-HMGB1 siRNAs (DsiRNA), scrambled RNA (negative control, NC), HPRT1 DsiRNA (positive control) and a fluorescent transfection efficiency control (TYE563) were purchased (Integrated DNA Technologies Inc., Coralville, IA) to maximize the probability of achieving successful HMGB1 knockdown. Lipofectamine 2000 (ThermoFisher) was used to transfect DsiRNA into the NHBE cells. We have listed the sequences of siRNAs and NC siRNA in the Supplementary table 1.

To carry out transfection with various siRNAs, NHBE cells were first cultured in the BEGM without antibiotics. For each transfection, 1 nM of (DsiRNA) for HMGB1, scrambled siRNA (negative control), HPRT1 DsiRNA (positive control) and a fluorescent transfection control (TYE563) were diluted in Opti-MEM media and gently mixed with Lipofectamine 2000 according to the manufacturer's instructions and protocols as per a published

manuscript (Chang et al. 2012). Following incubation for 20 min at room temperature, the transfection mixture was added to the cells and the cells were further incubated at 37°C for 24 hours. Knockdown was authenticated by qRT-PCR and western blot analysis of the target gene and protein, respectively (Supplementary fig. 1). Transfection was verified by fluorescent microscopy for TYE563 (fluorescent transfection control) and images were acquired using Nikon Eclipse TE2000-U inverted fluorescence microscope (Nikon, Tokyo, Japan). Images were processed using HCLImage live 4 software (Hamamatsu Corporation, Sewickley, PA).

Cell viability assay and MTT assay

Before executing each experiment, cell viability was quantified. Live/dead cell count was determined by 4% trypan blue dye (EMD Millipore) exclusion and percentage viability was calculated. The population of cells with more than 95% viability was used for the experiments.

The MTT assay has been commonly used in the estimation of LC₅₀ and cell viability by measuring the formazan produced when mitochondrial dehydrogenase enzymes cleave the tetrazolium ring (Latchoumycandane et al. 2005). We used the MTT assay to determine the LC₅₀ of the treatment groups in NHBE cells listed in Figure 1a and 1b. Cells were seeded (20,000 cells/well) in a 96-well culture plate and treated for 24 hours and 8 hours/day for 5 days. After the treatment, the cells were washed with PBS and incubated with 200 µl of 0.25% (w/v) MTT in BEGM for 3 hours at 37°C. The supernatant was removed, and MTT crystals were solubilized in 200 µl of dimethyl sulfoxide. Mitochondrial activity was measured by quantifying fluorescence using SpectraMax spectrophotometer (Molecular Devices Corporation) at 570 nm with the reference wavelength at 630 nm.

Transmission Electron Microscopy

For transmission electron microscopy (TEM), cells were seeded (1×10^6 cells/well) in 12-well plates with Poly D-lysine hydrobromide (Sigma-Aldrich, St. Louis, MO) coated coverslips and chronically exposed to the treatments as outlined in Figure 1b. Post-treatment NHBE cells were washed twice with DPBS and fixed with 3% glutaraldehyde (w/v) and 1% paraformaldehyde (w/v) in 0.1M cacodylate buffer, pH 7.4 for 48 hours at 4°C. Coverslips were rinsed 3 times in 0.1M cacodylate buffer and then post-fixed in 1% osmium tetroxide in 0.1 M cacodylate buffer for 1 hour (room temp.) The samples were rinsed in deionized distilled water and en bloc stained with 2% aqueous uranyl acetate for 30 min., dehydrated in a graded ethanol series, cleared with ultra-pure acetone, infiltrated and embedded using EmBed (EPON) formula epoxy resin (Electron Microscopy Sciences, Ft. Washington, PA) by inverting onto BEEM® capsules. Resin blocks were polymerized for 48 hours at 65°C. Coverslips were separated from the resin by using liquid nitrogen, trapping the cell monolayer in the resin. Thick and ultrathin sections were prepared using a Leica UC6 ultramicrotome (North Central Instruments, Minneapolis, MN). Ultrathin sections were collected onto the copper grids and images were captured using a JEOL 2100 scanning and transmission electron microscope (Japan Electron Optic Laboratories, Peabody, MA) with a Gatan OneView 4K camera (Gatan inc., Pleasanton, CA).

Immunofluorescence microscopy

NHBE cells were seeded (1×10^6 cells/well) in 12-well plates with Poly D-lysine hydrobromide (Sigma-Aldrich, St. Louis, MO) coated coverslips and exposed to the treatments as outlined in Figure 1a and 1b. At the respective time points, the media was removed, and cells were washed with 1x PBS. Cells were fixed with 4% paraformaldehyde in PBS for 20 minutes at room temperature and washed with PBS. Cells were blocked for an hour using a blocking solution containing 10% normal donkey serum (EMD Millipore, Burlington, MA), 0.2% triton X 100 and PBS. Coverslips with cells were incubated with anti-HMGB1 (1:1000 dilution, rabbit polyclonal) antibody in antibody diluent solution (2.5% normal donkey serum, 0.25% sodium azide, 0.2% triton X 100, PBS) (AbCam, Cambridge, MA) with overnight incubation at 4° C. Next, coverslips were incubated with donkey anti-rabbit biotin-conjugated secondary antibody (1:400, diluted in antibody diluent, HMGB1) (Jackson ImmunoResearch, West Grove, PA) for an hour at room temperature. Next, 1:300 dilution of streptavidin Cy3 in PBS (HMGB1) was added. Coverslips were mounted onto slides using VECTASHIELD antifade mounting medium with 4',6-Diamidino-2-Phenylindole, Dihydrochloride (DAPI, Vector Labs, Burlingame, CA) and images were captured using Nikon Eclipse TE2000-U inverted fluorescence microscope (Nikon, Tokyo, Japan). Images were processed using HCSImage live 4 software (Hamamatsu Corporation, Sewickley, PA).

Subcellular fractionation

Whole-cell and subcellular protein lysate extractions (cytosol and MT) were conducted at 4°C using cold reagents. For whole-cell protein lysates, cell pellets were subjected to lysis using RIPA buffer with HALT protease and phosphatase inhibitor (ThermoFisher Scientific). Subcellular fractionation of cell pellets for isolation of mitochondria was carried out using the Mitochondria Isolation Kit for Cultured Cells (ThermoFisher Scientific) as per the manufacturer's instructions. The cytosolic fraction and isolated mitochondria were lysed with RIPA buffer [with protease and phosphatase inhibitors] for 30 min at 4°C and periodic sonication on ice, followed by centrifugation to collect lysate. Protein concentrations of the fractions were quantified by Bradford assay (Bio-Rad) and stored at -80°C until use.

mtDNA isolation and long-range PCR

To find out mitochondrial DNA (mtDNA) leakage into cellular cytosol, mtDNA was isolated from mitochondria-free cytosolic fraction of the cells using the Genomic DNA Purification kit (ThermoFisher Scientific) as per the manufacturer's instructions. The purity and concentration of the isolated DNA was quantified using NanoVue Plus spectrophotometer (GE Healthcare, UK). Due to low concentrations, the mtDNA was first amplified using long-range PCR and the primers used are listed in Supplementary table 2. PCR reactions were performed at 94°C for 1 min followed by 30 cycles at 98°C for 10 s, 60°C for 40 s, 68°C for 16 min and a final elongation for 10 min (Liu et al. 2015). The presence of mtDNA was confirmed by separating the PCR product by electrophoresis on a 0.8% agarose gel stained with ethidium bromide. We ensured that there was equal amounts of template mtDNA in each sample (for qPCR reaction) by adjusting the concentration of amplified mtDNA that was obtained.

Real Time – qPCR

Total RNA was isolated using TRIzol extraction methods (Seo et al. 2014) and RNA concentration was measured using NanoVue Plus spectrophotometer (GE Healthcare, UK). One µg of RNA was used to synthesize cDNA using the High-Capacity cDNA Reverse Transcription Kit (ThermoFisher Scientific) following the manufacturer's instructions. qRT-PCR was performed using 500 ng of cDNA in a 10 µL reaction volume for each target in triplicates. The housekeeping genes 16S rRNA (for mtDNA fold change) and 18S rRNA (ThermoFisher Scientific) were used. No-template controls and dissociation curves were run for all reactions to exclude cross-contamination. The primers for genes of interest listed in Supplementary table 2 were synthesized at Iowa State University's DNA Facility. The qRT-PCR reactions were run in a QuantiStudio-3™ (ThermoFisher Scientific) detection system and the data was analyzed using 2^{-CT} method (Livak and Schmittgen).

Targeted gene array

qRT-PCR using TaqMan® Gene Expression Assays (Life Technologies, Carlsbad, CA) was performed for the 96 targets specific for human mitochondrial energy metabolism listed in Supplementary table 3. 500 ng of cDNA in a 10 µL reaction volume was prepared for each target in duplicates. The reaction conditions were as follows: 50°C for 2 minutes, 95°C for 2 minutes, followed by 40 cycles at 95°C for 1 second, and 60°C for 20 seconds. Data analysis was performed using the relative quantification app on ThermoFisher cloud and analyzed using 2^{-CT} method (Livak and Schmittgen 2001). The genes with a fold change of 10 and 10 were selected and represented on a heat map. Using the Kyoto Encyclopedia of Genes and Genomes (KEGG) database, upregulated and downregulated pathways with significantly altered mRNA transcripts with FDR corrected p-value cut-off <0.05 were selected and represented by gene counts.

Western blot analysis

Lysates (whole cell, cytosol and mt containing equal amounts of protein (20 µg/sample), along with a molecular weight marker (Bio-Rad), were run on 10–15% sodium dodecyl sulfate/polyacrylamide gel electrophoresis (SDS-PAGE) as previously described (Bhat et al. 2019). Proteins were transferred to a nitrocellulose membrane and nonspecific binding sites were blocked with Licor Odyssey blocking buffer. The membranes were then incubated with different primary antibodies and dilutions listed in Supplementary table 4. Next, membranes were incubated with one of the following secondary antibodies: Alexa Fluor 680 goat anti-mouse, Alexa Fluor 680 donkey anti-rabbit, or IRDye 800CW donkey anti-rabbit (1:10,000; LI-COR) listed in Supplementary table 5. To confirm equal protein loading, blots were probed with relevant housekeeping proteins listed in Supplementary table 4. Western blot images were captured using Odyssey® CLx IR imaging system (LI-COR Biotechnology) and analysis was performed using ImageJ program (National Institutes of Health).

Intracellular reactive oxygen species

Intracellular reactive oxygen species (ROS) production was measured using chloromethyl derivative of dichlorodihydrofluorescein diacetate (CM-H₂DCFDA) (ThermoFisher Scientific, USA). A working solution of 10 µM of DCFDA in DPBS was used. NHBE

cells (50,000 cells/well) were seeded in a 96 well plate and incubated in a 5% CO₂ incubator to reach confluence. The cells were incubated with CM-H₂DCFDA working solution at 37°C for 30 min, following treatments as outlined in Figure 1a. The cells were then washed and fluorescence intensity of the oxidized form of H₂DCFDA was measured at excitation/emission wavelengths of 488/535 nm using SpectraMax spectrophotometer (Molecular Devices Corporation). The results were expressed as mean fluorescence intensity relative to control.

Mitochondrial activity and mitochondrial superoxide

NHBE cells were seeded (50,000 cells/well) in a 96-well culture plate and treated as outlined in Figure 1a and 1b. Following treatment, the media was removed and 100 µl of MitoTracker green (200 nM) and MitoSOX red (5 µM) dye diluted in BEGM was added into each well and incubated at 37°C for 15 min. Following incubation, the cells were washed with DPBS and fluorescence intensity was measured by spectrophotometer reading taken at excitation/emission wavelengths of 485/520 nm and 510/580 nm, respectively, SpectraMax spectrophotometer (Molecular Devices Corporation). The results were expressed as percentage fluorescence relative to control.

NHBE cells were also seeded (1×10⁶ cells/well) in 12-well plates with Poly D-lysine hydrobromide (Sigma-Aldrich, St. Louis, MO) coated coverslips and exposed to the treatments as outlined in Figure 1a and 1b. At the respective time points, the media was removed, and cells were washed with DPBS. These were stained with MitoTracker Red CMXRos (200 nM) and incubated at 37°C for 15 min. The cells were washed with DPBS and fixed with 4% paraformaldehyde in PBS for 20 minutes at room temperature and washed with PBS again. Coverslips were mounted onto slides using VECTASHIELD antifade mounting medium with 4',6-Diamidino-2-Phenylindole, Dihydrochloride (DAPI, Vector Labs, Burlingame, CA) and imaged using Nikon Eclipse TE2000-U inverted fluorescence microscope (Nikon, Tokyo, Japan). Images were processed using HCLImage live 4 software (Hamamatsu Corporation, Sewickley, PA).

Mitochondrial glucose uptake

Cellular glucose uptake by NHBE cells was measured using fluorescent d-glucose analog 2-[N-(7-nitrobenz-2-oxa-1,3-diazol-4-yl) amino]-2-deoxy-D-glucose (2-NBDG) (Zou et al. 2005). Cells were seeded (50,000 cells/well) in a 96-well culture plate and treated as outlined in Figure 1a and 1b. After treatment, the media was removed and 100 µL of 50 µg/mL 2-FITC labeled NBDG in BEGM was added into each well and incubated at 37°C for 20 min. Following incubation, the cells were washed with DPBS and fluorescence intensity was measured by spectrophotometer reading taken at an at excitation/emission wavelengths of 465/540 nm using SpectraMax spectrophotometer (Molecular Devices Corporation). The results were expressed as percentage fluorescence relative to control.

Mitochondrial calcium influx

Mitochondrial calcium influx ([Ca²⁺]_{mito}) in NHBE cells was measured using the Rhod-2AM dye. After treatment, the mitochondria were isolated using the Mitochondria Isolation Kit for Cultured Cells (ThermoFisher Scientific). Using Bradford assay, we

measured the protein concentration so as to maintain consistency in the number of mitochondria loaded into the wells of a 96-well plate. A protein concentration of 100 µg was loaded into each well and Rhod-2AM (Abcam, 10 µM) dye was added and incubated at 37°C for 30 minutes to stain the mitochondria. The plate was later read at an excitation/emission wavelengths of 552/581 nm using SpectraMax spectrophotometer (Molecular Devices Corporation).

NHBE cells were also seeded (1×10^6 cells/well) in 12-well plates with Poly D-lysine hydrobromide (Sigma-Aldrich, St. Louis, MO) coated coverslips and exposed to the treatments as outlined in Figure 1a and 1b. At the respective time points, the media was removed, and cells were washed with DPBS. These were stained with Rhod-2AM (Abcam, 10 µM) and incubated at 37°C for 30 min. The cells were washed with DPBS and fixed with 4% paraformaldehyde in PBS for 20 minutes at room temperature and washed with PBS again. Coverslips were mounted onto slides using VECTASHIELD antifade mounting medium with 4',6-Diamidino-2-Phenylindole, Dihydrochloride (DAPI, Vector Labs, Burlingame, CA) and imaged using EVOS M5000 imaging system (ThermoFisher Scientific).

Griess assay

Griess assay was performed as described (Gordon et al. 2011). Concentration of secreted nitric oxide was measured (representing reactive nitrogen species (RNS)) as nitrite levels in cell culture media using Griess reagent (Sigma-Aldrich) and sodium nitrite standard curve, prepared using a stock solution of 200 µM. The assay was performed in a 96 well-plate and absorbance was measured at 550 nm using SpectraMax spectrophotometer (Molecular Devices Corporation). The results were expressed as µM concentration of nitrite secreted.

Trans-epithelial electrical resistance (TEER)

TEER is the potential difference across the epithelium, which is a measure of the tightness of the cell-cell contacts within the epithelium and TEER is measured using a pair of electrodes (Srinivasan et al. 2015). NHBE cells were plated on 10.5mm trans-well inserts in a 12 well plate and allowed to grow. Cell confluence was monitored by TEER measurements with the Epithelial Voltohmmeter 2 (EVOM2, WPI, Sarasota, FL). The value obtained is an indication of the integrity of the epithelial cell monolayers. Once TEER value reached a steady state, treatments outlined in Figure 1a were added to the apical surface of the cells and TEER measurements were performed every 12 hours for 5 days. The mean of four measurements per insert was calculated. The electrical resistance of inserts without cells was subtracted from all samples, and the resistance values obtained was multiplied with the surface area of the inserts for measuring the TEER values ($\Omega \cdot \text{cm}^2$).

Statistical analysis

Data analysis was performed using GraphPad Prism 8.0 software (La Jolla, CA, USA). Raw data were analyzed with either Student's t-test or using one-way ANOVA, and Tukey's post hoc test was performed to compare all the treatment groups. A p-value of < 0.05 was considered statistically significant. *p < 0.05, **p < 0.01, ***p < 0.001, ****p < 0.0001 and

* indicates different from control. Samples for all the assays were derived from the same experiment and were processed in parallel.

RESULTS

Endotoxin levels in ODE samples

Endotoxin activity of the diluted ODE samples (1:10) is listed in Table 1. From the seven samples, we found that endotoxin values ranged from 0.8067 ± 0.0008 to 1.433 ± 0.02 EU/mL (Table 1). Sample # 7 (endotoxin level 1.263 ± 0.7 EU/mL) was used for all experiments listed in this manuscript.

Suppression of HMGB1 expression in ODE exposed NHBE cells promotes mitochondrial fission

To assess the impact of HMGB1 on mitochondria, primary NHBE cells were transfected with HMGB1 targeted siRNA to induce knockdown. Successful transfection was first confirmed by using a fluorescently tagged DsiRNA (DsiRNA TYE 563; 10 nmol) that produced positive immunofluorescence in the cytoplasm of NHBE cells at 24 h post-transfection (Supplementary fig. 1a–a''). After establishing an optimal transfection protocol, NHBE cells were transfected with three HMGB1 targeting siRNA sequences (R1, R2, and R3; 10 nmol each) and a negative control siRNA (scrambled DsiRNA; 10 nmol) and incubated for 24 h. The knockdown was confirmed by western blot and qPCR of samples from all the groups. Quantified data showed a decrease in HMGB1 levels for all three sequences and no change in the negative control (Supplementary fig. 1b–d). The siRNA sequence that induced the highest percentage of knockdown (siRNA.R3) was selected to perform all the experiments.

NHBE cells with and without HMGB1 knockdown were exposed to either media (control) or ODE for 24 h (Fig. 1a). mRNA fold change of HMGB1 was measured and was found to increase on ODE exposure but remained low in cells with HMGB1 knockdown (Supplementary fig. 1e). The impact of lack of HMGB1 on mitochondrial morphology was investigated. On ODE exposure, the expression of mitochondrial fusion proteins mitofusin 1 (MFN1), mitofusin 2 (MFN2), and optic atrophy 1 (OPA1) were measured. The expression of MFN1 and MFN2 decreased in NHBE cells with and without HMGB1 exposed to ODE, while OPA1 levels were significantly upregulated in NHBE cells treated with ODE alone (Fig. 2a–f). Mitochondrial fission protein, dynamin-related protein 1 (DRP1), level was significantly upregulated in the ODE exposed cells lacking in HMGB1 (Fig. 2g, h). To further corroborate whether the mitochondrial morphological changes observed are associated with the number of active mitochondria, change in mitochondrial mass was measured by quantifying mitotracker green fluorescence. There was a significant decrease in the mitochondrial mass on exposure to ODE in cells with and without HMGB1 (Fig. 2i). ODE exposed cells stained with mitotracker red dye were visualized to accurately identify the morphological changes. In NHBE cells treated with ODE alone, the mitochondrial network appeared filamentous and branched with few fragmented or globular mitochondria (Fig. 2j'). By contrast, mitochondria appeared more fragmented or globular in ODE exposed NHBE cells lacking HMGB1 indicating mitochondrial fission (Fig. 2j'').

ODE exposure increases BNIP3 expression in NHBE cells

We examined whether the lack of HMGB1 during ODE exposure impacts mitochondria-targeted autophagy, referred to as mitophagy. The expression of the two important mediators of mitophagy, PTEN-induced kinase 1 (PINK1) and the E3 ubiquitin protein ligase Parkin, were measured. NHBE cells treated with ODE for 24 h showed no change in PINK1 but significantly decreased Parkin expression (Fig. 3a–d). ODE-exposed NHBE cells lacking HMGB1 showed a significant decrease in both PINK1 and Parkin on exposure to ODE. The expression of BNIP3, a mitochondrial Bcl-2 Homology 3 (BH3)-only protein, known to activate mitochondrial permeability transition (MPT) was also measured (Ney 2015). BNIP3 levels were significantly increased on exposure to ODE alone, while cells treated with anti-HMGB1 siRNA showed a decrease in the expression of BNIP3 (Fig. 3e, f).

ODE exposure induces mtDNA release into extracellular fluid

Using qPCR, we measured the levels of mtDNA released into the mt-free cytosol and cell culture supernatant (extracellular spaces) samples. NHBE cells treated with ODE for 24 h showed a significant increase in mtDNA levels both in the mt-free cytosol and supernatant samples, while ODE exposed cells lacking HMGB1 had decreased levels in both cytosol and supernatant samples (Fig. 4a, b). In addition, ODE exposed cells showed increased expression of TLR9, a receptor that mediates cellular response to unmethylated CpG dinucleotides found in bacterial DNA and eukaryotic mtDNA to mount an innate immune response (Fig. 4c, d). Next, we examined whether the mtDNA released from the mitochondrial matrix is activating the cGAS-STING pathway. Although no significant change in cyclic GMP-AMP synthase (cGAS) and interferon regulatory factor 3 (IRF3) expression were observed, a significant increase in interferon gamma inducible protein 16 (IFI16) protein expression in cells treated with ODE alone was documented (Fig. 4e–j). In ODE exposed cells lacking HMGB1, the levels of these proteins were comparable to controls or significantly decreased in the case of IRF3 (Fig. 4i, j). mRNA fold change of type 1 interferons, *ifna1*, *ifna4*, and *ifnb*, which are downstream targets of IFI16 and IRF3, was measured. Cells exposed to ODE for 24 h showed a significant increase in the mRNA levels of *ifna1*, *ifna4*, and *ifnb*, while the levels remained comparable to controls in cells lacking HMGB1 (Fig. 4k–m).

To investigate whether mtDNA is released during repeated exposure of ODE, NHBE cells were treated with media alone (control) or ODE (1%) followed by media (control) or HMGB1 neutralization antibody (10 µg/mL) for 8 h per day for five days (Fig. 1b). Following a 5-day exposure there was an increase in cytosolic mtDNA content in cells treated with HMGB1 neutralization antibody and an increase in extracellular mtDNA in cells treated with ODE alone (Supplementary fig. 2a, b). There was also an increase in *ifna4* and a decrease in *ifna* and *ifnb* mRNA levels in cells treated with HMGB1 neutralization antibody (Supplementary fig. 2c–e).

Mitochondrial biogenesis is promoted in ODE exposed NHBE cells lacking HMGB1

Mitochondrial biogenesis in NHBE cells was assessed by measuring Peroxisome proliferator-activated receptor gamma coactivator 1-alpha (PGC1α) and Nuclear factor erythroid 2-related factor 2 (NRF2) protein expression. NHBE cells with and without

HMGB1 exposed to ODE for 24 h showed a significant increase in PGC1 α and NRF2 expression compared to controls (Fig. 5a–d). Expression of TFAM, a downstream target of PGC1 α and NRF2, in both the mitochondria and mitochondria-free cytosol was measured. In ODE exposed NHBE cells lacking HMGB1, we noted a small decrease in TFAM levels in the mitochondria (~10%) and an increase in the cytosolic levels (~10%) (Fig. 5e–g). We observed that the cytosolic levels of TFAM significantly decreased in cells treated with ODE alone (Fig. 5e, g). mRNA fold change of downstream targets of NRF2, Glutathione S-transferase P (*gstp1*), heme oxygenase 1 (*hmox1*), and NAD(P)H Quinone Dehydrogenase 1 (*nqo1*), was measured. In ODE exposed NHBE cells lacking HMGB1, we documented a significant decrease in *gstp1*, while we noted an increase in mRNA levels of *hmox1* and *nqo1*. In ODE treated cells, while no significant change was observed in the expression of *gstp1*, a significant increase was observed in *hmox1* and *nqo1*, when compared to control and cells lacking HMGB1 (Fig. 5h–j).

On the other hand, in the repeated long-term exposure model, we observed that ODE induced a significant decrease in mRNA fold change of *pgc1a* and *nrf2*, and HMGB1 neutralization significantly increased *pgc1a* and *nrf2* levels. However, HMGB1 neutralization did not increase the levels to that of controls. (Supplementary fig. 3a–b). mRNA fold change of *tfam* is significantly reduced as well (Supplementary fig. 3c). mRNA levels of *nqo1* was significantly reduced, while that of *hmox1* increased in both treatments (Supplementary fig. 3d–e).

Single ODE exposure leads to release of cytochrome c

To assess the impact of the increased mtDNA leakage, we measured the release of other mitochondrial DAMPs (mtDAMPs) and reactive species generation. In addition to TFAM and mtDNA, cytochrome c is another prominent mtDAMP which is a key player in apoptosis (Cai et al. 1998; Ott et al. 2002). We measured the expression of cytochrome c in mitochondrial and mitochondria-free cytosolic fractions of NHBE cells. ODE exposure of NHBE cells increased the cytosolic cytochrome c levels but not the mitochondrial cytochrome c levels (Fig. 6a–c). ODE exposed cells lacking HMGB1 showed a significant decrease in both mitochondrial and cytosolic cytochrome c protein levels. Griess assay results showed an increase in RNS levels on exposure to ODE, with levels comparable to control in cells lacking HMGB1 (Fig. 6d). To corroborate this, we measured the mRNA fold change in *nos2*, the gene coding for inducible nitric oxide synthase (iNOS) and observed an increased expression in cells treated with ODE alone while *nos2* mRNA fold change decreased in cells lacking HMGB1 (Fig. 6e). In addition, we documented an increase in intracellular reactive oxygen species (ROS) levels in ODE treated cells, which was significantly decreased in cells lacking HMGB1 (Fig. 6f). On the other hand, the mitochondrial superoxide levels were significantly decreased in both cases compared to control (Fig. 6g). We observed a decrease in mitochondrial calcium levels ($[Ca^{2+}]_{mito}$) in cells exposed to ODE alone whereas $[Ca^{2+}]_{mito}$ levels increased in cells lacking HMGB1 (Fig. 6h) (Fig. 6i', i'''). In the repeated ODE exposure model, ODE exposure alone decreased the ($[Ca^{2+}]_{mito}$) whereas neutralization of HMGB1 increased the ($[Ca^{2+}]_{mito}$) (Supplementary fig. 4a–a''') (Supplementary fig. 4b). There was no change in the levels of mitochondrial superoxide (Supplementary fig. 4c).

Repeated ODE exposure promotes mitochondrial fusion

Using transmission electron microscopy (TEM), we assessed the ultrastructural changes in NHBE cells following exposure to ODE with or without HMGB1 neutralization for 8 h/day for 5 days (Fig. 1b). Compared to controls, ODE-treated NHBE cells showed change in mitochondrial morphology. Mitochondria appeared to be more elongated with cristolysis and in some cases there was mitochondrial hypertrophy (Fig. 7a, a'). In contrast, neutralization of HMGB1 decreased the ODE-induced cristolysis and mitochondrial shape resembled that of controls (Fig. 7a, a''). We stained the cells with mitotracker dye to assess changes in the number of active mitochondria. Mitotracker stained cells revealed no change in mitochondrial mass among any of the treatments (Fig. 7c). However, we did observe noticeable ODE-induced changes in mitochondrial morphology. Compared to controls, ODE exposed NHBE cells showed filamentous mitochondria and mitochondria appeared to be more clustered close to the nucleus (Fig. 7b, b'). With HMGB1 neutralization, the mitochondria were more fragmented and globular, and were less clustered near the nuclei when compared to ODE exposed cells (Fig. 7b''). Using MTT assay we measured the cell viability and HMGB1 neutralization rescued the ODE-induced decrease in cell viability (Fig. 7d).

HMGB1 neutralization rescues mitochondrial respiration in repeated ODE exposure models

A targeted analysis of expression of genes associated with mitochondrial respiration was performed. A pre-designed gene array with 96 genes (including housekeeping genes) specific to various components involved in mitochondrial respiration was used and fold changes were measured by qPCR (Supplementary table 3). The change in gene expression between ODE exposed NHBE cells, with or without HMGB1 neutralization for 8 h/day for 5 days, was calculated relative to control by the 2^{-CT} method and genes with a fold change ≥ 10 or ≤ 10 were represented on a heat map (Livak and Schmittgen 2001). Neutralization of HMGB1 increased the expression of genes of protein subunits involved in mitochondrial respiration such as various subunits of ATP synthase (*atp*), cytochrome c oxidase (*cox*), ubiquinol-cytochrome c reductase (*uqcr*) and NADH:ubiquinone oxidoreductase (*naduf*) when compared to ODE treated cells (Fig. 8a). Using the Kyoto Encyclopedia of Genes and Genomes (KEGG) database, upregulated and downregulated pathways associated with mitochondria bioenergetics were analyzed (Fig. 8b–e). Pathways related to the metabolism, respiratory electron transport, and mitochondria biogenesis which were downregulated with ODE exposure were significantly upregulated on HMGB1 neutralization (Fig. 8c, d).

Single ODE exposure induces hypoxia response in NHBE cells lacking HMGB1

Oxygen sensing and adaptations in NHBE cells (with or without anti-HMGB1 siRNA treatment) exposed to ODE for 24 h was measured. An increase in hypoxia-inducible factor 1-alpha (HIF1 α) protein expression was observed in cells lacking HMGB1 while the expression of HIF1 α was significantly reduced with ODE exposure alone (Fig. 9a, b). mRNA fold change of ubiquitin ligase Von Hippel-Lindau tumor suppressor (*vhl*) was significantly increased in both ODE exposed NHBE cells with or without HMGB1 (Fig. 9c). mRNA fold change of genes involved in glucose uptake, solute carrier family 2 member 6

(*slc2a6*), and glycolysis, enolase 1 (*eno1*), was measured. A significant increase in *slc2a6* in both ODE exposed cells with or without HMGB1 was observed, whereas *eno1* was upregulated in cells lacking HMGB1 (Fig. 9d, e). To corroborate this, we measured cellular glucose uptake potential and glycolytic activity in ODE exposed NHBE cells by culturing cells with the glucose analog 2-NBDG. Here a significant increase in the uptake of 2-NBDG was observed in ODE exposed cells lacking HMGB1, while exposure to ODE alone significantly decreased 2-NBDG uptake (Fig. 9f).

We compared the expression of the factors involved in hypoxia and glucose uptake in NHBE cells in the repeated ODE exposure model. mRNA fold change of *hif1a* and *vhl* was significantly decreased in ODE exposed cells but remained unchanged in cells with HMGB1 neutralization (Fig. 10a, b). There was no significant change in the expression of *slc2a6* in any of the treatments. However, the expression of *eno1* was significantly downregulated in ODE exposed cells (Fig. 10c, d). 2-NBDG uptake was decreased in ODE exposed cells and was comparable to control in cells treated with HMGB1 neutralization antibody (Fig. 10e).

HMGB1 neutralization increased tight junction integrity in ALI cultures of NHBE cells

NHBE cells were seeded onto a semi-permeable membrane to develop an air-liquid interface (ALI) culture model and exposed to ODE, with or without HMGB1 neutralization for 1 h/day for 5 days (Fig. 1c). mRNA fold change of forkhead box J1 (*foxj1*) and its downstream target cilia and flagella associated protein 157 (*cfap157*) was measured (Fig. 11a, b). Exposure of cells to ODE alone showed a significant increase in fold change of both genes, while the expression was comparable to control in ODE exposed cells with HMGB1 neutralization. Tight junction integrity was determined by measuring the mRNA fold change of occludin (*ocln*) and claudin 1 (*cldn1*), and by quantifying the trans-epithelial electrical resistance (TEER). mRNA fold change of *ocln* and *cldn1* was significantly downregulated in ODE exposed cells, while on HMGB1 neutralization *ocln* levels were comparable to control and *cldn1* was significantly decreased (Fig. 11c, d). TEER measurements were performed to identify the impact of ODE on tight junction integrity. A decrease in TEER values (electrical resistance) is proportional to decreased tight junction integrity. TEER values were significantly decreased on exposure to ODE as early as 12 h and continued to decrease with time compared to control. On the other hand, although a similar decrease was observed with the neutralization of HMGB1 at 12 h, TEER values remained steady after day 1 post-exposure and were not rescued significantly (Fig. 11e).

DISCUSSION

The prevalence of airway inflammatory diseases in agricultural workers is high, where the development of a myriad of respiratory symptoms has been documented (Poole and Romberger 2012). Our previous work confirmed that OD exposure results in airway epithelial damage independent of a functional TLR4 receptor indicating the importance PAMPs other than endotoxin or LPS (Charavaryamath et al. 2008). Further, our recent work in an *in vitro* monocytic cell line model confirmed that OD exposure induces cellular stress and mitochondrial damage (Mahadev Bhat et al. 2021). Recent studies have shown the relationship between induction of mitochondrial dysfunction and several

inflammatory airway diseases such as asthma and chronic obstructive pulmonary disease (COPD) (Schumacker et al. 2014; Prakash et al. 2017; Aghapour et al. 2019; Cloonan et al. 2020). Our past work and other published work provide a strong premise for examining the role of mt-dysfunction in airway epithelial models of OD-exposure.

High mobility group box 1 (HMGB1) protein, an essential protein which during inflammatory conditions acts as a DAMP in airway inflammatory conditions such as COPD, cigarette smoke exposure and acute lung injury (Rubartelli and Lotze 2007; Zhang et al. 2010; Pouwels et al. 2014; Yang et al. 2015, p. 1; Ugrinova and Pasheva 2017). Previously we have shown how HMGB1 behaves as a pro-inflammatory mediator in ODE exposed cells and how antibody-mediated neutralization of secreted HMGB1 decreases the inflammatory cytokines, ROS and RNS, and had an overall protective effect at 24 to 48 h post-treatment (Bhat et al. 2019; Massey et al. 2019). In the current study, we investigated the impact of secreted HMGB1 on ODE-induced mitochondrial dysfunction in NHBE cell models of single and repeated five-day exposure. Overall, we demonstrate that blocking HMGB1 secretion induces mitochondrial fragmentation, mitochondrial biogenesis and an increase in mitochondrial respiration. These responses were consistent across the single (acute) exposure, with siRNA knockdown of HMGB1, as well as in repeated (chronic) exposure to ODE, with antibody-mediated HMGB1 neutralization.

In the present study, we used two *in vitro* models, a 24 h ODE exposure (single, acute) with siRNA mediated knockdown of HMGB1 (Table 5.2a) and a 5-day (8 h/day) ODE exposure (repeated, chronic) with antibody-mediated HMGB1 neutralization to examine exposure-induced mitochondrial dysfunction. The siRNA-mediated knockdown of HMGB1 is suitable for single (acute) exposure as the suppression of mRNA and protein lasts for about 72 hours. Therefore, we used an antibody-mediated neutralization approach in our repeated (five-day) exposure model.

Mitochondrial remodeling is mediated by the balance between MFN1/2 and DRP1, which promoted mitochondrial fusion and fission, respectively (Song et al. 2009; Liesa et al. 2009; Palmer et al. 2011; Ranieri et al. 2013; Huang et al. 2018). Our results from single exposure showed that ODE decreases the expression of MFN1 and MFN2 in cells with and without HMGB1, but OPA1 expression in cells lacking HMGB1 was significantly decreased. OPA1 is a dynamin-related GTPase that has been shown to mediate inner mitochondrial membrane (IMM) fusion, while MFN1/2 mediate the fusion of the outer mitochondrial membrane (OMM) (Song et al. 2009; MacVicar and Langer 2016). OPA1 in particular, has been identified as a significant player in the regulation of various mitochondrial functions, sLoss of OPA1 has been shown to induce DRP1-dependent mitochondrial fragmentation (Lee et al. 2004). This was observed in our results where siRNA-mediated HMGB1 knockdown increased the DRP1 expression in ODE exposed cells. The fusion of mitochondria is dependent on dimerization of mitofusin proteins, MFN1 and MFN2. Thus the decreased MFN1/2 expression in ODE exposed cells lacking HMGB1 explains the increase in mitochondrial fragmentation (Chen et al. 2003; Song et al. 2009; Liesa et al. 2009; Palmer et al. 2011; Ranieri et al. 2013). Overall, our results highlight that lack of HMGB1 has an impact on OPA1 but not on MFN1/2.

Next, we used 2D fluorescence imaging and transmission electron microscopy (TEM) to evaluate mitochondrial morphology and ultrastructural changes in both acute and repeated exposure *in vitro* models. First, we observed that single exposure of cells with or without HMGB1 reduced the mitochondrial mass. When visualized, cells with HMGB1 when exposed to ODE showed a filamentous and branched network of mitochondria with few fragmented and globular mitochondria. Interestingly, cells that lacked HMGB1 displayed increased fragmentation and globular mitochondria upon exposure to ODE. These results indicate that ODE exposure induced mitochondrial changes become pronounced with the loss of nuclear HMGB1, underscoring the importance of nuclear HMGB1 in maintaining the health of the cellular mitochondria (Tang et al. 2011). Our TEM images confirmed that ODE exposure induces mitochondrial elongation, cristolysis and hypertrophy, whereas HMGB1 neutralization reduced the ODE-induced cristolysis and mitochondria appeared healthy. Further, neutralization of HMGB1 induced a globular morphology of mitochondria with elongated cristae running parallel to the longitudinal axis of the mitochondria. Overall, ODE-induced mitochondrial fusion observed in our study could be a cellular stress response aimed at compensating for the loss of important mitochondrial functions (Chen et al. 2003; Landes et al. 2010; Westrate et al. 2014; Eisner et al. 2018; Tilokani et al. 2018). Our recent using microglial model confirms the ODE exposure-induced cristolysis and the morphological basis of exposure-induced decreases in mt-bioenergetics (Massey et al. 2021).

One of the consequences associated with mitochondrial fragmentation is the loss of mitochondrial membrane potential and mitophagy. We investigated the mitochondrial clearance (mitophagy) and involvement of PINK1-Parkin signaling pathway. ODE exposed NHBE cells showed no significant change in PINK1 expression, while Parkin was significantly decreased and NHBE cells lacking HMGB1 showed reduced levels of both PINK1 and Parkin. These results indicate that the observed fragmentation of mitochondria in cells lacking HMGB1 could be due to active mitochondrial biogenesis (Ding and Yin 2012). We also measured the expression of BNIP3, a mitochondrial transmembrane protein known to have pro-death activity and a role in activating mitochondrial permeability transition (MPT). Here we observed an increase in BNIP3 expression on ODE exposure, whereas, in cells lacking HMGB1, the BNIP3 levels return to baseline (control) levels. The increase in BNIP3 expression could be promoting permeability of the inner and outer mitochondrial membranes resulting in increased ROS production, release of cytochrome c and mitochondrial depolarization, all of which together initiates cellular apoptosis (Kim et al. 2002; Ney 2015). Considering the increase in OPA1 levels in ODE exposed cells, evidence suggests that BNIP3 interacts with OPA1 inhibiting OPA1-mediated fusion, in acute conditions, or disassembly of OPA1 complexes, in chronic conditions, leading to cellular death (Landes et al. 2010). This is further corroborated by the increase in cytosolic cytochrome C levels in 24 h ODE exposed cells. On the contrary, cytochrome C levels were decreased in cells lacking HMGB1 following exposure. The release cytochrome C in ODE exposed cells could be promoting increased ROS generation, caspase activation (caspase 3 and caspase 9), and eventually leading to apoptotic cell dismantling (Cai et al. 1998; Ott et al. 2002; Quinsay et al. 2010).

One of the major consequences of increased MPT during cellular stress is the release of mitochondrially derived molecules referred to as mtDAMPs (García and Chávez 2007; Zhang et al. 2010; Quinsay et al. 2010; Nakahira et al. 2011). Fragmented mtDNA released from the damaged mitochondria is one of the critical mtDAMPs which regulates innate immune responses (Lee and Wei 2005; West et al. 2015; Ploumi et al. 2017). Release of mitochondrial DNA into the cytoplasm and out into the extracellular milieu activates multiple pattern recognition receptors and innate immune responses, including cGAS-STING, TLR9, and inflammasome formation leading to, among others, robust type I interferon responses (Cloonan and Choi 2012; West et al. 2015; Chen et al. 2016). The results of the present study show an increase in cytosolic and extracellular mitochondrial DNA copy number in NHBE cells exposed to ODE for 24 h, which is reduced in ODE exposed cells lacking HMGB1 indicating how HMGB1 regulates mt-damage and release of mtDNA. Concurrently we also observed an increase in the expression of TLR9, IFI16, IRF3, and type 1 interferon, which could be leading to cell death. On the other hand, during chronic ODE exposure we document an increase in the cytosolic mtDNA on HMGB1 neutralization, but not extracellularly, and an increase in only *ifna4* mRNA, indicating that the neutralization of HMGB1 could be promoting mitochondrial biogenesis.

Mitochondrial reactive oxygen species (mtROS) is the most universal and well-studied mtDAMP and is a by-product of mitochondrial respiration and ATP production (Zorov et al. 2014). NHBE cells exposed to ODE for 24 h show an increase in intracellular ROS while the levels of mtROS remain low in all the treatment groups. The ODE-mediated increase in intracellular ROS is consistent with our previous findings, where it is known to initiate the inflammatory cascade (Bhat et al. 2019; Massey et al. 2019). The lack of increase in mtROS could be another indicator of mitochondrial biogenesis in play. Thus, the observed mitochondrial fragmentation in cells lacking HMGB1 or with antibody-mediated HMGB1 neutralization may reflect an important adaptive response to protect the mitochondria from an increase in ROS production and oxidative stress with ODE exposure. In addition to this, we also document an increase in mitochondrial calcium influx in ODE treated cells lacking HMGB1 or with antibody-mediated HMGB1 neutralization. This increase in mitochondrial calcium influx could be promoting mitochondrial O₂ consumption and ATP synthesis, as well as mitochondrial metabolism (Rizzuto et al. 2000; Parekh 2003; Brookes et al. 2004; Hajnóczky et al. 2007; Finkel et al. 2015).

Mitochondrial biogenesis, along with mitophagy, allow cells to quickly replace metabolically dysfunctional mitochondria before reaching the stage of energy failure. The results of our study provide converging evidence that 24 h ODE exposure of cells with HMGB1 or cells without HMGB1 induce mitochondrial biogenesis. First, we observed an increase in PGC1 α expression in cells exposed to ODE, with or without HMGB1. The role of PGC1 α in regulating mitochondrial biogenesis has been well established (Wu et al. 1999; Handschin and Spiegelman 2006; Triantafyllidis et al. 2007). We then measured the expression of NRF2 and observed a similar increase as that of PGC1 α . NRF2 is known to regulate the expression of the electron transport chain subunits and binds to the promoter regions of genes involved in the transcription of mtDNA. NRF2 is known to be regulated by its transcriptional coactivator PGC1 α , which together induces the expression of TFAM thus activating mitochondrial biogenesis. In line with this, we observe an increase in TFAM

protein expression in mitochondria-free cytosolic fractions of 24 h ODE exposed cells lacking HMGB1. However, we observed that a repeated 5-day ODE exposure resulted in significantly lower levels of the gene expression of PGC1 α , NRF2, and TFAM when compared to the controls with and without HMGB1 neutralization.

The extent of mitochondrial dysfunction is determined by the level of negative impact on mitochondrial respiration and metabolism. In our study, we found that NHBE cells repeatedly exposed to ODE display a distinctive mitochondrial gene profile, where we observe a downregulation of genes associated with mitochondrial metabolism, citric acid (TCA) cycle, OXPHOS, and mitochondrial biogenesis. This is consistent with the increased levels of ROS, induction of MPT and mtDNA release on ODE exposure. With the neutralization of HMGB1, we document an increase in the fold change of genes coding the protein subunits associated with mitochondrial electron transport chain (ETC), such as ATP, COX, NADUF and UQCR. In line with this, we show evidence of ODE-mediated decrease in cellular glucose uptake and glycolytic ability in both acute and chronic exposure models, while lack of or neutralization of HMGB1 increased the cellular glucose uptake and glycolytic ability. This metabolic profile in NHBE cells may have a direct impact on the maintenance of overall lung homeostasis and function on exposure to ODE *in vivo* (Wu et al. 1999; Koopman et al. 2005; Dranka et al. 2011; Agrawal and Mabalirajan 2015). Our results provide a robust framework for the future *in vivo* experiments.

Reduced oxygen availability elicited by hypoxia and mitochondrial dysfunction leads to increased production of ROS by the electron transport chain (ETC) (Baik and Jain 2020). The observed ODE-exposure induced hypoxia response could be well explained based on the increased intracellular ROS production and downregulation of ETC. Interestingly, we observed a decrease in HIF1 α expression in 24 h ODE exposed NHBE cells while it increased in cells lacking HMGB1, indicative of hypoxia. Thus, lack of HMGB1 acts as protective through activation of HIF1 α . This is supported by the cellular studies showing that HIF1 α activation could rescue the effects of ETC deficiency in mitochondrial diseases (Jain et al. 2016). Hypoxia may be triggering a HIF-dependent transcriptional program activating key pathways promoting glycolysis, ATP production and decreased ROS generation. This would also be reducing the levels of O₂ being taken up by the cell which would, in turn, decrease the availability of substrate for free radical production and aberrant cellular signaling. We observed that, HMGB1 neutralization resulted in the normoxic conditions in the repeated ODE exposure model. Hence, we can theorize that short-term hypoxic conditions may be beneficial in reversing mitochondrial dysfunction.

In addition, using an ALI model of ODE exposure, we investigated the impact of HMGB1 on tight junction integrity. Previously we have shown the impact of 24 h ODE exposure on tight junction expression *in vivo*, but the role of HMGB1 remains to be investigated (Shrestha et al. 2021). In this study, we observe a significant decrease in transepithelial electrical resistance (TEER) with repeated ODE exposure as early as 12 hours post-exposure. Although HMGB1 neutralization does not reverse the effect of ODE on tight junction integrity, the TEER values plateau and remain unchanged one day post-exposure. The neutralization of HMGB1 does not significantly rescue ODE-induced decrease in TEER. However, there is a certain amount of protection of epithelial integrity. This was

corroborated by the measurement of claudin-1 and occludin, indicating that ODE exposure directly affects the tight junction integrity. Although this is valid preliminary evidence on the impact of ODE on tight junction integrity, thorough *in vivo* work needs to be performed to confirm this finding.

In summary, the results of the present study indicate that targeting HMGB1 in ODE induced inflammatory process promotes mitochondrial biogenesis and metabolism by promoting hypoxic conditions and decreasing ROS production (Fig. 12). It is likely that blocking HMGB1 release following ODE exposure leads to a coordinated adaptive response in NHBE cells involving mitochondrial fragmentation, increased mitochondrial biogenesis, and mitochondrial metabolism. As a result, the maximum O₂ consumption and ROS production per mitochondrion are reduced, while the demand for ATP synthesis is still met. Future studies using HMGB1 airway epithelial cell-specific conditional knock-out mice or systemic neutralization of HMGB1 may unravel further mechanistic basis of targeting HMGB1 in rescuing ODE-induced mitochondrial deficits.

Supplementary Material

Refer to Web version on PubMed Central for supplementary material.

Acknowledgments

We would like to thank Tracey Stewart at Iowa State University's Roy J. Carver High Resolution Microscopy Facility for assistance with transmission electron microscopy. We would like to thank Dr. Kevin Tracey (Feinstein Institutes for Medical Research, Northwell Health, NY) for providing us with the anti-HMGB1 neutralization antibody and Dr. Y.S. Prakash (Mayo Clinic, Rochester, MN) and Dr. K. L. Bailey (UNMC, Omaha, NE) for providing us with normal human bronchial epithelial cells when needed. We would also like to thank the department of biomedical sciences and Dr. M. Cho at Iowa State University for providing us with access to necessary equipment. We would like to thank Drs. Thippeswamy and Kanthasamy (Biomedical Sciences) for access to equipment and facilities.

Funding

C.C. laboratory is funded through startup grant through Iowa State University, a pilot grant (5 U54 OH007548) from CDC-NIOSH (Centers for Disease Control and Prevention-The National Institute for Occupational Safety and Health) and a seed grant through CVM (College of Veterinary Medicine) at the Iowa State University.

Nomenclature

OD	Organic Dust
ODE	Organic Dust Extract
NHBE	Normal Human Bronchial Epithelial
BEGM	Bronchial Epithelial Growth Medium
ALI	Air Liquid Interface
HMGB1	High Mobility Group Box 1
RAGE	Receptor for advanced glycation end products
TLR	Toll-like receptor

NOD2	Nucleotide-binding Oligomerization Domain-containing 2
ATP	Adenosine Triphosphate
OXPHOS	Oxidative Phosphorylation
TFAM	mitochondrial Transcription Factor A
COX	Cytochrome C Oxidase
mtND1	mitochondrial NADH dehydrogenase 1
TEM	Transmission Electron Microscopy
DMSO	Dimethyl Sulfoxide

REFERENCES

- Aghapour M, Remels AHV, Pouwels SD, et al. (2019) Mitochondria: at the crossroads of regulating lung epithelial cell function in chronic obstructive pulmonary disease. *American Journal of Physiology-Lung Cellular and Molecular Physiology* 318:L149–L164. 10.1152/ajplung.00329.2019 [PubMed: 31693390]
- Agrawal A, Mabalirajan U (2015) Rejuvenating cellular respiration for optimizing respiratory function: targeting mitochondria. *American Journal of Physiology-Lung Cellular and Molecular Physiology* 310:L103–L113. 10.1152/ajplung.00320.2015 [PubMed: 26566906]
- An J, Jr H, Aj N, et al. (2020) MyD88 regulates a prolonged adaptation response to environmental dust exposure-induced lung disease. *Respir Res* 21:97–97. 10.1186/s12931-020-01362-8 [PubMed: 32321514]
- Andersson U, Tracey KJ (2011) HMGB1 Is a Therapeutic Target for Sterile Inflammation and Infection. *Annu Rev Immunol* 29:139–162. 10.1146/annurev-immunol-030409-101323 [PubMed: 21219181]
- Baik AH, Jain IH (2020) Turning the Oxygen Dial: Balancing the Highs and Lows. *Trends in Cell Biology* 30:516–536. 10.1016/j.tcb.2020.04.005 [PubMed: 32386878]
- Bailey KL, Poole JA, Mathisen TL, et al. (2008) Toll-like receptor 2 is upregulated by hog confinement dust in an IL-6-dependent manner in the airway epithelium. *American Journal of Physiology-Lung Cellular and Molecular Physiology* 294:L1049–L1054. 10.1152/ajplung.00526.2007 [PubMed: 18359883]
- Bhat SM, Massey N, Karriker LA, et al. (2019) Ethyl pyruvate reduces organic dust-induced airway inflammation by targeting HMGB1-RAGE signaling. *Respiratory Research* 20:27. 10.1186/s12931-019-0992-3 [PubMed: 30728013]
- Brookes PS, Yoon Y, Robotham JL, et al. (2004) Calcium, ATP, and ROS: a mitochondrial love-hate triangle. *American Journal of Physiology-Cell Physiology* 287:C817–C833. 10.1152/ajpcell.00139.2004 [PubMed: 15355853]
- Cai J, Yang J, Jones DeanP (1998) Mitochondrial control of apoptosis: the role of cytochrome c. *Biochimica et Biophysica Acta (BBA) - Bioenergetics* 1366:139–149. 10.1016/S0005-2728(98)00109-1 [PubMed: 9714780]
- Cantaert T, Baeten D, Tak PP, van Baarsen LG (2010) Type I IFN and TNF α cross-regulation in immune-mediated inflammatory disease: basic concepts and clinical relevance. *Arthritis Research & Therapy* 12:219. 10.1186/ar3150 [PubMed: 21062511]
- Chang K, Marran K, Valentine A, Hannon GJ (2012) RNAi in Cultured Mammalian Cells Using Synthetic siRNAs. *Cold Spring Harb Protoc* 2012:pdb.prot071076. 10.1101/pdb.prot071076
- Charavaryamath C, Juneau V, Suri SS, et al. (2008) Role of Toll-like receptor 4 in lung inflammation following exposure to swine barn air. *Exp Lung Res* 34:19–35. 10.1080/01902140701807779 [PubMed: 18205075]

- Charavaryamath C, Singh B (2006) Pulmonary effects of exposure to pig barn air. *J Occup Med Toxicol* 1:10. 10.1186/1745-6673-1-10 [PubMed: 16756675]
- CHAUNG WW, WU R JI Y, et al. (2012) Mitochondrial transcription factor A is a proinflammatory mediator in hemorrhagic shock. *Int J Mol Med* 30:199–203. 10.3892/ijmm.2012.959 [PubMed: 22469910]
- Chen H, Detmer SA, Ewald AJ, et al. (2003) Mitofusins Mfn1 and Mfn2 coordinately regulate mitochondrial fusion and are essential for embryonic development. *J Cell Biol* 160:189–200. 10.1083/jcb.200211046 [PubMed: 12527753]
- Chen Q, Sun L, Chen ZJ (2016) Regulation and function of the cGAS–STING pathway of cytosolic DNA sensing. *Nature Immunology* 17:1142–1149. 10.1038/ni.3558 [PubMed: 27648547]
- Cloonan SM, Choi AM (2012) Mitochondria: commanders of innate immunity and disease? *Current Opinion in Immunology* 24:32–40. 10.1016/j.coi.2011.11.001 [PubMed: 22138315]
- Cloonan SM, Choi AMK (2016) Mitochondria in lung disease. *J Clin Invest* 126:809–820. 10.1172/JCI81113 [PubMed: 26928034]
- Cloonan SM, Kim K, Esteves P, et al. (2020) Mitochondrial dysfunction in lung ageing and disease. *European Respiratory Review* 29: 10.1183/16000617.0165-2020
- Ding W-X, Yin X-M (2012) Mitophagy: mechanisms, pathophysiological roles, and analysis. *Biol Chem* 393:547–564. 10.1515/hsz-2012-0119 [PubMed: 22944659]
- Dranka BP, Benavides GA, Diers AR, et al. (2011) Assessing bioenergetic function in response to oxidative stress by metabolic profiling. *Free Radical Biology and Medicine* 51:1621–1635. 10.1016/j.freeradbiomed.2011.08.005 [PubMed: 21872656]
- Eisner V, Picard M, Hajnóczky G (2018) Mitochondrial dynamics in adaptive and maladaptive cellular stress responses. *Nature Cell Biology* 20:755–765. 10.1038/s41556-018-0133-0 [PubMed: 29950571]
- Fetterman JL, Sammy MJ, Ballinger SW (2017) Mitochondrial Toxicity of Tobacco Smoke and Air Pollution. *Toxicology* 391:18–33. 10.1016/j.tox.2017.08.002 [PubMed: 28838641]
- Finkel T, Menazza S, Holmström KM, et al. (2015) The Ins and Outs of Mitochondrial Calcium. *Circ Res* 116:1810–1819. 10.1161/CIRCRESAHA.116.305484 [PubMed: 25999421]
- García N, Chávez E (2007) Mitochondrial DNA fragments released through the permeability transition pore correspond to specific gene size. *Life Sciences* 81:1160–1166. 10.1016/j.lfs.2007.08.019 [PubMed: 17870132]
- Gordon R, Hogan CE, Neal ML, et al. (2011) A simple magnetic separation method for high-yield isolation of pure primary microglia. *J Neurosci Methods* 194:287–296. 10.1016/j.jneumeth.2010.11.001 [PubMed: 21074565]
- Hajnóczky G, Saotome M, Csordás G, et al. (2007) Calcium Signalling and Mitochondrial Motility. In: *Mitochondrial Biology: New Perspectives*. John Wiley & Sons, Ltd, pp 105–121
- Handschin C, Spiegelman BM (2006) Peroxisome Proliferator-Activated Receptor γ Coactivator 1 Coactivators, Energy Homeostasis, and Metabolism. *Endocrine Reviews* 27:728–735. 10.1210/er.2006-0037 [PubMed: 17018837]
- Huang C-Y, Chiang S-F, Chen WT-L, et al. (2018) HMGB1 promotes ERK-mediated mitochondrial Drp1 phosphorylation for chemoresistance through RAGE in colorectal cancer. *Cell Death & Disease* 9:1–15. 10.1038/s41419-018-1019-6 [PubMed: 29298988]
- Jain IH, Zazzeron L, Goli R, et al. (2016) Hypoxia as a therapy for mitochondrial disease. *Science* 352:54–61. 10.1126/science.aad9642 [PubMed: 26917594]
- Julian MW, Shao G, Vangundy ZC, et al. (2013) Mitochondrial transcription factor A, an endogenous danger signal, promotes TNF α release via RAGE- and TLR9-responsive plasmacytoid dendritic cells. *PLoS ONE* 8:e72354. 10.1371/journal.pone.0072354
- Kelly KJ, Poole JA (2019) Pollutants in the workplace: Effect on occupational asthma. *Journal of Allergy and Clinical Immunology* 143:2014–2015. 10.1016/j.jaci.2019.04.013 [PubMed: 31029774]
- Kim J-Y, Cho J-J, Ha J, Park J-H (2002) The Carboxy Terminal C-Tail of BNip3 Is Crucial in Induction of Mitochondrial Permeability Transition in Isolated Mitochondria. *Archives of Biochemistry and Biophysics* 398:147–152. 10.1006/abbi.2001.2673 [PubMed: 11831844]

- Koopman WJH, Visch H-J, Verkaar S, et al. (2005) Mitochondrial network complexity and pathological decrease in complex I activity are tightly correlated in isolated human complex I deficiency. *American Journal of Physiology-Cell Physiology* 289:C881–C890. 10.1152/ajpcell.00104.2005 [PubMed: 15901599]
- Landes T, Emorine LJ, Courilleau D, et al. (2010) The BH3-only Bnip3 binds to the dynamin Opa1 to promote mitochondrial fragmentation and apoptosis by distinct mechanisms. *EMBO reports* 11:459–465. 10.1038/embor.2010.50 [PubMed: 20436456]
- Latchoumycandane C, Anantharam V, Kitazawa M, et al. (2005) Protein kinase Cdelta is a key downstream mediator of manganese-induced apoptosis in dopaminergic neuronal cells. *J Pharmacol Exp Ther* 313:46–55. 10.1124/jpet.104.078469 [PubMed: 15608081]
- Lee H-C, Wei Y-H (2005) Mitochondrial biogenesis and mitochondrial DNA maintenance of mammalian cells under oxidative stress. *The International Journal of Biochemistry & Cell Biology* 37:822–834. 10.1016/j.biocel.2004.09.010 [PubMed: 15694841]
- Lee Y, Jeong S-Y, Karbowski M, et al. (2004) Roles of the Mammalian Mitochondrial Fission and Fusion Mediators Fis1, Drp1, and Opa1 in Apoptosis. *MBoC* 15:5001–5011. 10.1091/mbc.e04-04-0294 [PubMed: 15356267]
- Liesa M, Palacín M, Zorzano A (2009) Mitochondrial Dynamics in Mammalian Health and Disease. *Physiological Reviews* 89:799–845. 10.1152/physrev.00030.2008 [PubMed: 19584314]
- Liu J, Fang H, Chi Z, et al. (2015) XPD localizes in mitochondria and protects the mitochondrial genome from oxidative DNA damage. *Nucleic Acids Res* 43:5476–5488. 10.1093/nar/gkv472 [PubMed: 25969448]
- Livak KJ, Schmittgen TD (2001) Analysis of Relative Gene Expression Data Using Real-Time Quantitative PCR and the 2⁻CT Method. *Methods* 25:402–408. 10.1006/meth.2001.1262 [PubMed: 11846609]
- MacVicar T, Langer T (2016) OPA1 processing in cell death and disease – the long and short of it. *J Cell Sci* 129:2297–2306. 10.1242/jcs.159186 [PubMed: 27189080]
- Mahadev Bhat S, Shrestha D, Massey N, et al. (2021) Organic dust exposure induces stress response and mitochondrial dysfunction in monocytic cells. *Histochem Cell Biol*. 10.1007/s00418-021-01978-x
- Massey N, Puttachary S, Bhat SM, et al. (2019) HMGB1-RAGE Signaling Plays a Role in Organic Dust-Induced Microglial Activation and Neuroinflammation. *Toxicol Sci* 169:579–592. 10.1093/toxsci/kfz071 [PubMed: 30859215]
- Massey N, Shrestha D, Bhat SM, et al. (2021) Organic dust-induced mitochondrial dysfunction could be targeted via cGAS-STING or cytoplasmic NOX-2 inhibition using microglial cells and brain slice culture models. *Cell Tissue Res*. 10.1007/s00441-021-03422-x
- May S, Romberger DJ, Poole JA (2012) Respiratory Health Effects of Large Animal Farming Environments. *J Toxicol Environ Health B Crit Rev* 15:524–541. 10.1080/10937404.2012.744288 [PubMed: 23199220]
- Nakahira K, Haspel JA, Rathinam VAK, et al. (2011) Autophagy proteins regulate innate immune responses by inhibiting the release of mitochondrial DNA mediated by the NALP3 inflammasome. *Nature Immunology* 12:222–230. 10.1038/ni.1980 [PubMed: 21151103]
- Nath Neerukonda S, Mahadev-Bhat S, Aylward B, et al. (2018) Kinome analyses of inflammatory responses to swine barn dust extract in human bronchial epithelial and monocyte cell lines. *Innate Immun* 24:366–381. 10.1177/1753425918792070 [PubMed: 30092684]
- Ney PA (2015) Mitochondrial autophagy: Origins, significance, and role of BNIP3 and NIX. *Biochimica et Biophysica Acta (BBA) - Molecular Cell Research* 1853:2775–2783. 10.1016/j.bbamcr.2015.02.022 [PubMed: 25753537]
- Nordgren TM, Charavaryamath C (2018) Agriculture Occupational Exposures and Factors Affecting Health Effects. *Curr Allergy Asthma Rep* 18:65. 10.1007/s11882-018-0820-8 [PubMed: 30291457]
- Ott M, Robertson JD, Gogvadze V, et al. (2002) Cytochrome c release from mitochondria proceeds by a two-step process. *PNAS* 99:1259–1263. 10.1073/pnas.241655498 [PubMed: 11818574]

- Palmer CS, Osellame LD, Stojanovski D, Ryan MT (2011) The regulation of mitochondrial morphology: Intricate mechanisms and dynamic machinery. *Cellular Signalling* 23:1534–1545. 10.1016/j.cellsig.2011.05.021 [PubMed: 21683788]
- Parekh AB (2003) Mitochondrial Regulation of Intracellular Ca²⁺ Signaling: More Than Just Simple Ca²⁺ Buffers. *Physiology* 18:252–256. 10.1152/nips.01458.2003
- Piantadosi CA, Suliman HB (2017) Mitochondrial Dysfunction in Lung Pathogenesis. *Annual Review of Physiology* 79:495–515. 10.1146/annurev-physiol-022516-034322
- Ploumi C, Daskalaki I, Tavernarakis N (2017) Mitochondrial biogenesis and clearance: a balancing act. *The FEBS Journal* 284:183–195. 10.1111/febs.13820 [PubMed: 27462821]
- Poole JA, Barnes CS, Demain JG, et al. (2019) Impact of weather and climate change with indoor and outdoor air quality in asthma: A Work Group Report of the AAAAI Environmental Exposure and Respiratory Health Committee. *Journal of Allergy and Clinical Immunology* 143:1702–1710. 10.1016/j.jaci.2019.02.018 [PubMed: 30826366]
- Poole JA, Burrell AM, Wyatt TA, et al. (2010) NOD2 Negatively Regulates Organic Dust-Induced Inflammation in Monocytes/Macrophages. *Journal of Allergy and Clinical Immunology* 125:AB118. 10.1016/j.jaci.2009.12.467
- Poole JA, Romberger DJ (2012) Immunological and Inflammatory Responses to Organic Dust in Agriculture. *Curr Opin Allergy Clin Immunol* 12:126–132. 10.1097/ACI.0b013e3283511d0e [PubMed: 22306554]
- Poole JA, Wyatt TA, Essen SGV, et al. (2007) Repeat organic dust exposure-induced monocyte inflammation is associated with protein kinase C activity. *Journal of Allergy and Clinical Immunology* 120:366–373. 10.1016/j.jaci.2007.04.033 [PubMed: 17555806]
- Poole JA, Wyatt TA, Kielian T, et al. (2011) Toll-like receptor 2 regulates organic dust-induced airway inflammation. *Am J Respir Cell Mol Biol* 45:711–719. 10.1165/rcmb.2010-0427OC [PubMed: 21278324]
- Pouwels SD, Heijink IH, ten Hacken NH, et al. (2014) DAMPs activating innate and adaptive immune responses in COPD. *Mucosal Immunology* 7:215–226. 10.1038/mi.2013.77 [PubMed: 24150257]
- Prakash YS, Pabelick CM, Sieck GC (2017) Mitochondrial Dysfunction in Airway Disease. *CHEST* 152:618–626. 10.1016/j.chest.2017.03.020 [PubMed: 28336486]
- Qi L, Sun X, Li F-E, et al. (2015) HMGB1 Promotes Mitochondrial Dysfunction-Triggered Striatal Neurodegeneration via Autophagy and Apoptosis Activation. *PLoS One* 10: 10.1371/journal.pone.0142901
- Qin S, Wang H, Yuan R, et al. (2006) Role of HMGB1 in apoptosis-mediated sepsis lethality. *J Exp Med* 203:1637–1642. 10.1084/jem.20052203 [PubMed: 16818669]
- Quinsay MN, Lee Y, Rikka S, et al. (2010) Bnip3 mediates permeabilization of mitochondria and release of cytochrome c via a novel mechanism. *Journal of Molecular and Cellular Cardiology* 48:1146–1156. 10.1016/j.yjmcc.2009.12.004 [PubMed: 20025887]
- Ranieri M, Brajkovic S, Riboldi G, et al. (2013) Mitochondrial Fusion Proteins and Human Diseases. In: *Neurology Research International*. <https://www.hindawi.com/journals/nri/2013/293893/>. Accessed 27 Jan 2021
- Rizzuto R, Bernardi P, Pozzan T (2000) Mitochondria as all-round players of the calcium game. *The Journal of Physiology* 529:37–47. 10.1111/j.1469-7793.2000.00037.x [PubMed: 11080249]
- Romberger DJ, Bodlak V, Von Essen SG, et al. (2002) Hog barn dust extract stimulates IL-8 and IL-6 release in human bronchial epithelial cells via PKC activation. *Journal of Applied Physiology* 93:289–296. 10.1152/japplphysiol.00815.2001 [PubMed: 12070216]
- Rubartelli A, Lotze MT (2007) Inside, outside, upside down: damage-associated molecular-pattern molecules (DAMPs) and redox. *Trends in Immunology* 28:429–436. 10.1016/j.it.2007.08.004 [PubMed: 17845865]
- Schumacker PT, Gillespie MN, Nakahira K, et al. (2014) Mitochondria in lung biology and pathology: more than just a powerhouse. *American Journal of Physiology-Lung Cellular and Molecular Physiology* 306:L962–L974. 10.1152/ajplung.00073.2014 [PubMed: 24748601]
- Seo J, Ottesen EW, Singh RN (2014) Antisense Methods to Modulate Pre-mRNA Splicing. In: Hertel KJ (ed) *Spliceosomal Pre-mRNA Splicing: Methods and Protocols*. Humana Press, Totowa, NJ, pp 271–283

- Sethi RS, Schneberger D, Charavaryamath C, Singh B (2017) Pulmonary innate inflammatory responses to agricultural occupational contaminants. *Cell Tissue Res* 367:627–642. 10.1007/s00441-017-2573-4 [PubMed: 28168324]
- Shrestha D, Bhat SM, Massey N, et al. (2021) Pre-exposure to hydrogen sulfide modulates the innate inflammatory response to organic dust. *Cell Tissue Res*. 10.1007/s00441-020-03333-3
- Song Z, Ghochani M, McCaffery JM, et al. (2009) Mitofusins and OPA1 Mediate Sequential Steps in Mitochondrial Membrane Fusion. *MBoC* 20:3525–3532. 10.1091/mbc.e09-03-0252 [PubMed: 19477917]
- Srinivasan B, Kolli AR, Esch MB, et al. (2015) TEER measurement techniques for in vitro barrier model systems. *J Lab Autom* 20:107–126. 10.1177/2211068214561025 [PubMed: 25586998]
- Tang D, Kang R, Livesey KM, et al. (2011) High-Mobility Group Box 1 Is Essential for Mitochondrial Quality Control. *Cell Metabolism* 13:701–711. 10.1016/j.cmet.2011.04.008 [PubMed: 21641551]
- Tilokani L, Nagashima S, Paupe V, Prudent J (2018) Mitochondrial dynamics: overview of molecular mechanisms. *Essays Biochem* 62:341–360. 10.1042/EBC20170104 [PubMed: 30030364]
- Triantafyllidis T, Benard G, Begueret H, et al. (2007) Bronchial smooth muscle remodeling involves calcium-dependent enhanced mitochondrial biogenesis in asthma. *Journal of Experimental Medicine* 204:3173–3181. 10.1084/jem.20070956 [PubMed: 18056286]
- Ugrinova I, Pasheva E (2017) HMGB1 Protein: A Therapeutic Target Inside and Outside the Cell. *Adv Protein Chem Struct Biol* 107:37–76. 10.1016/bs.apcsb.2016.10.001 [PubMed: 28215228]
- Warren KJ, Dickinson JD, Nelson AJ, et al. (2019) Ovalbumin-sensitized mice have altered airway inflammation to agriculture organic dust. *Respiratory Research* 20:51. 10.1186/s12931-019-1015-0 [PubMed: 30845921]
- West AP, Khoury-Hanold W, Staron M, et al. (2015) Mitochondrial DNA stress primes the antiviral innate immune response. *Nature* 520:553–557. 10.1038/nature14156 [PubMed: 25642965]
- Westrate LM, Drocco JA, Martin KR, et al. (2014) Mitochondrial Morphological Features Are Associated with Fission and Fusion Events. *PLOS ONE* 9:e95265. 10.1371/journal.pone.0095265
- Whitsett JA, Alenghat T (2015) Respiratory epithelial cells orchestrate pulmonary innate immunity. *Nature Immunology* 16:27–35. 10.1038/ni.3045 [PubMed: 25521682]
- Wu Z, Puigserver P, Andersson U, et al. (1999) Mechanisms Controlling Mitochondrial Biogenesis and Respiration through the Thermogenic Coactivator PGC-1. *Cell* 98:115–124. 10.1016/S0092-8674(00)80611-X [PubMed: 10412986]
- Wunschel J, Poole JA (2016) Occupational agriculture organic dust exposure and its relationship to asthma and airway inflammation in adults. *J Asthma* 53:471–477. 10.3109/02770903.2015.1116089 [PubMed: 26785925]
- Yang H, Wang H, Chavan SS, Andersson U (2015) High Mobility Group Box Protein 1 (HMGB1): The Prototypical Endogenous Danger Molecule. *Mol Med* 21 Suppl 1:S6–S12. 10.2119/molmed.2015.00087 [PubMed: 26605648]
- Ye C, Choi J-G, Abraham S, et al. (2012) Human macrophage and dendritic cell-specific silencing of high-mobility group protein B1 ameliorates sepsis in a humanized mouse model. *PNAS* 109:21052–21057. 10.1073/pnas.1216195109 [PubMed: 23213216]
- Zhang Q, Raoof M, Chen Y, et al. (2010) Circulating mitochondrial DAMPs cause inflammatory responses to injury. *Nature* 464:104–107. 10.1038/nature08780 [PubMed: 20203610]
- Zhou H, Wang Y, Wang W, et al. (2009) Generation of Monoclonal Antibodies against Highly Conserved Antigens. *PLOS ONE* 4:e6087. 10.1371/journal.pone.0006087 [PubMed: 19564921]
- Zorov DB, Juhaszova M, Sollott SJ (2014) Mitochondrial Reactive Oxygen Species (ROS) and ROS-Induced ROS Release. *Physiol Rev* 94:909–950. 10.1152/physrev.00026.2013 [PubMed: 24987008]
- Zou C, Wang Y, Shen Z (2005) 2-NBDG as a fluorescent indicator for direct glucose uptake measurement. *Journal of Biochemical and Biophysical Methods* 64:207–215. 10.1016/j.jbbm.2005.08.001 [PubMed: 16182371]

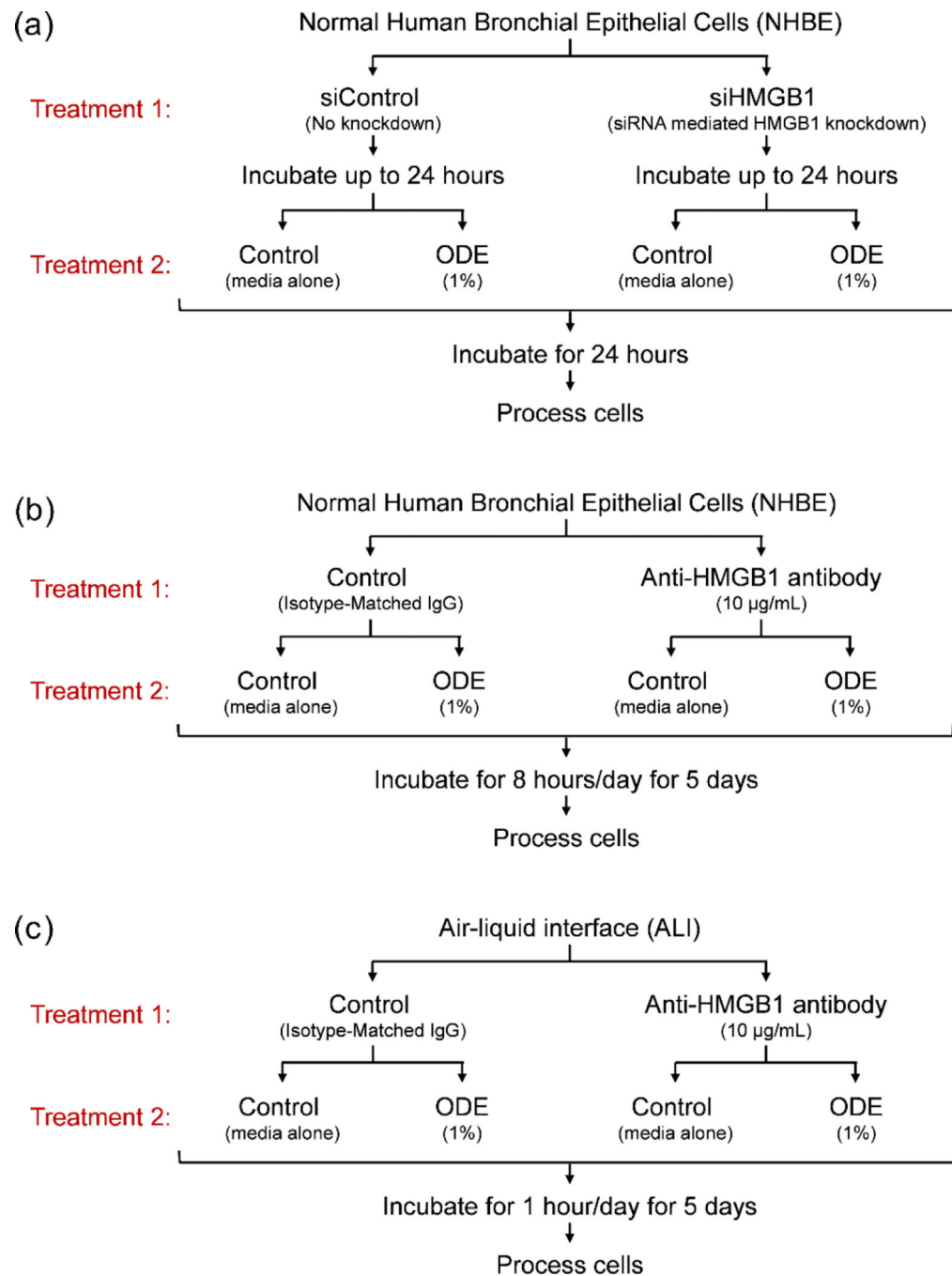


Fig. 1. ODE exposure of NHBE cells and air-liquid interface culture.

Three experimental designs were used to study the impact of HMGB1 on mitochondria during ODE exposure. For acute exposure, primary NHBE cells were transfected with HMGB1 targeted siRNA to induce knockdown followed by exposure to either media (control) or ODE (1%) for 24 h (a). For chronic exposure, NHBE cells were treated with media alone (control) or ODE (1%) followed by media (control) or HMGB1 neutralization antibody (10 µg/mL) for 8 h per day for five days (b). Air-liquid interface (ALI) culture model was developed by seeding NHBE cells onto a semi-permeable membrane to develop

and the differentiated cells were exposed to ODE, with or without HMGB1 neutralization for 1 h per day for 5 days (c).

Author Manuscript

Author Manuscript

Author Manuscript

Author Manuscript

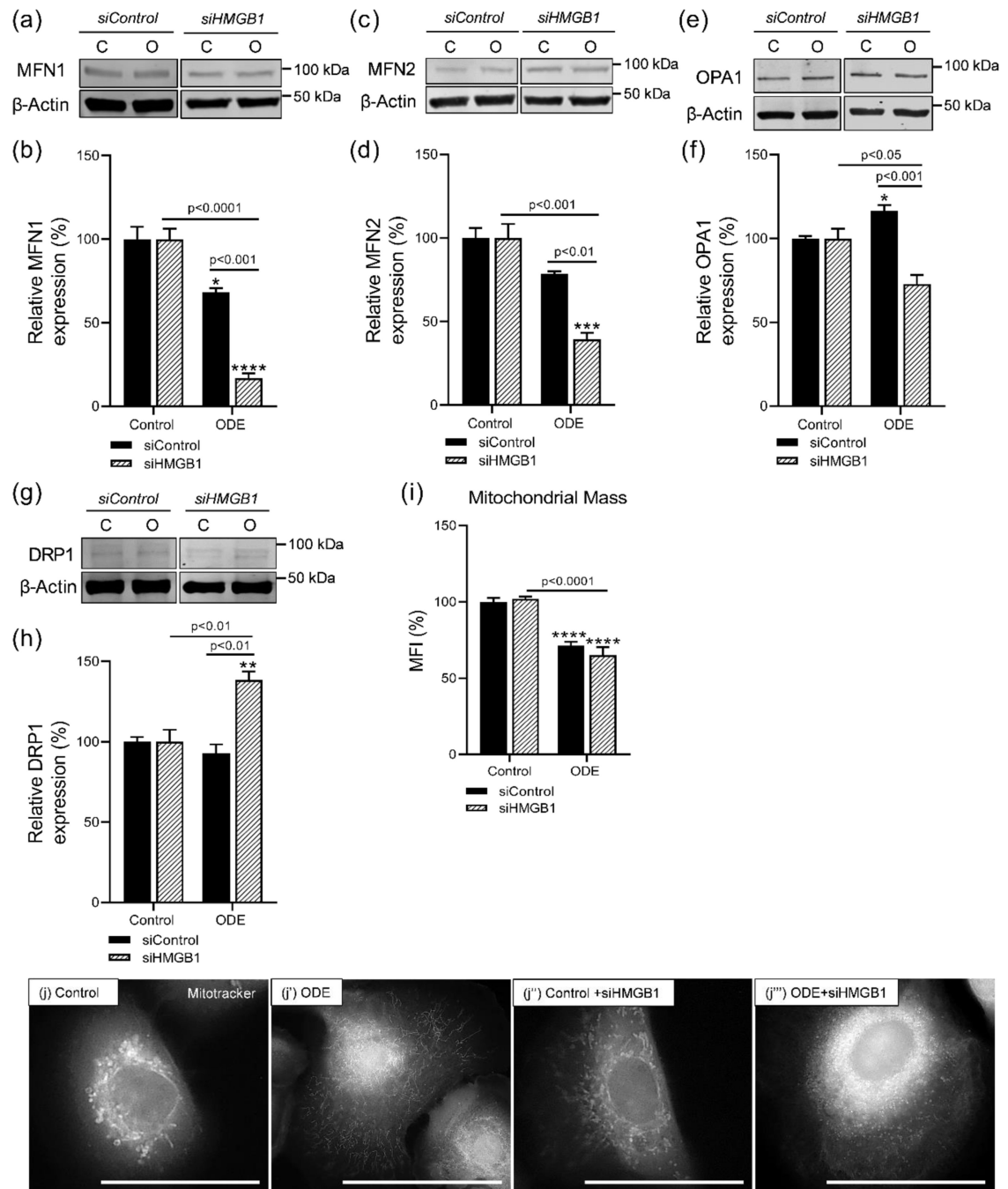


Fig. 2. HMGB1 knockdown promotes mitochondrial fission on OD exposure.

Changes in mitochondrial morphology in NHBE cells with or without siRNA mediated HMGB1 knockdown and treated with ODE (1%) for 24 h was assessed. Immunoblotting was performed to measure the mitochondrial fusion proteins MFN1 (a, b), MFN2 (c, d) and OPA1 (e, f) and fission protein DRP1 (g, h) and compared. Mitochondrial mass was measured (i) and the morphology was visualized by staining with Mito-tracker dye (j-j'''); Scale bar = 100 μ m). All the protein bands were normalized over β -actin (37 kDa) and percentage intensity relative to control was analyzed. Data was analyzed using one-way

ANOVA with Tukey's multiple comparison test (* $p < 0.05$, ** $p < 0.01$, *** $p < 0.001$, **** $p < 0.0001$) and represented as mean \pm SEM with $n = 3-6$ /treatment (* indicates significant difference from control).

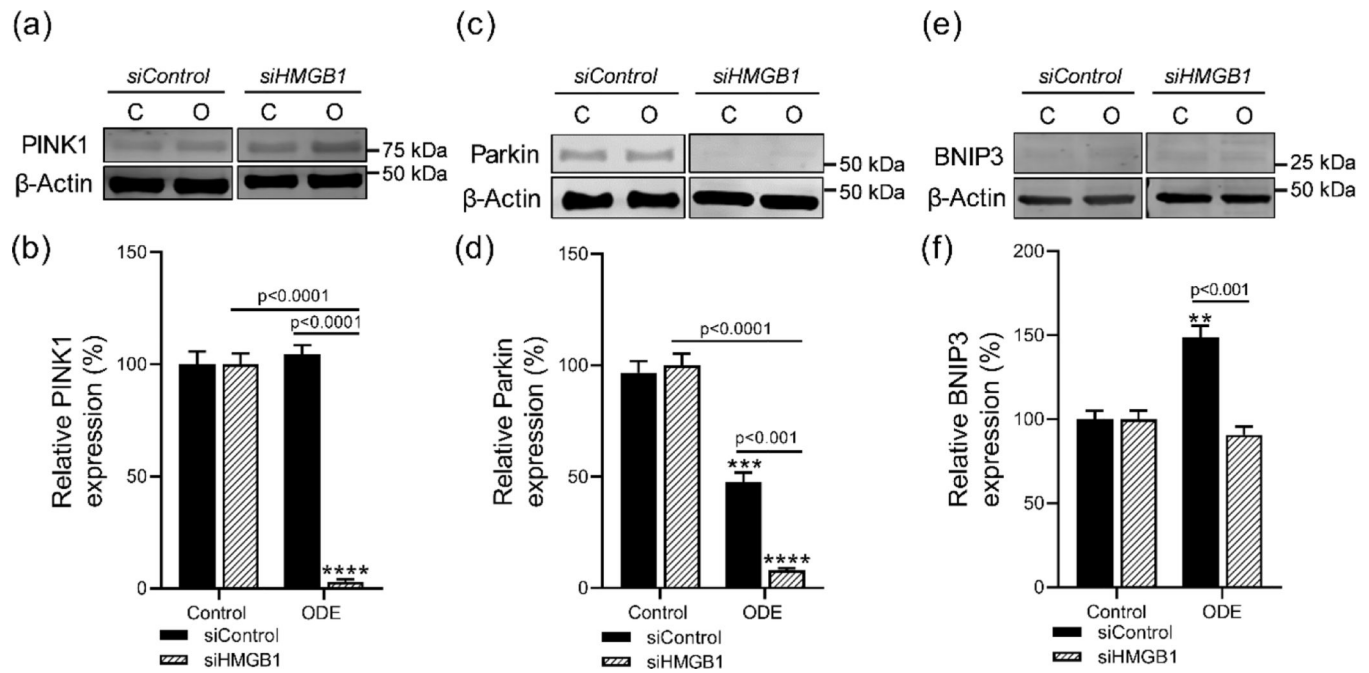


Fig. 3. OD exposure promotes apoptosis in NHBE cells.

Immunoblotting of NHBE cells, with or without siRNA mediated HMGB1 knockdown and treated with ODE (1%) for 24 h, was performed to measure expression of mitophagy markers, PINK1 (a, b) and Parkin (c, d), and BNIP3 (e, f). All the protein bands were normalized over β -actin (37 kD) and percentage intensity relative to control was analyzed. Data was analyzed using one-way ANOVA with Tukey's multiple comparison test (* $p < 0.05$, ** $p < 0.01$, *** $p < 0.001$, **** $p < 0.0001$) and represented as mean \pm SEM with $n = 3$ /treatment (* indicates significant difference from control).

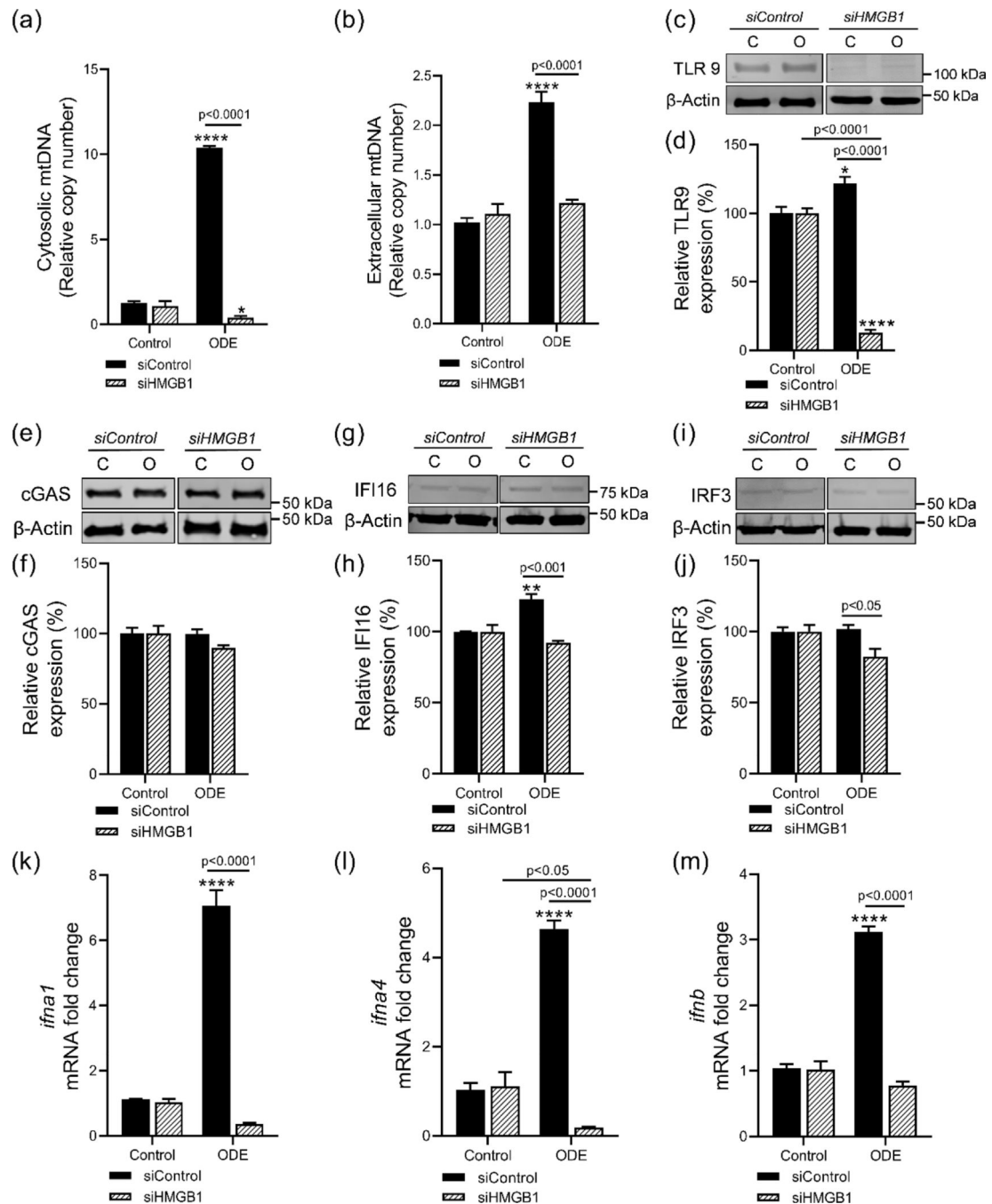


Fig. 4. Acute OD exposure mediated release of mtDNA stimulates IFN production.

Mitochondrial DNA (mtDNA) leakage into the cytosol (a) and extracellularly (b) in NHBE cells, with or without siRNA mediated HMGB1 knockdown and treated with ODE (1%) for 24 h was analyzed via qPCR. Immunoblotting was performed to measure expression of TLR9 (c, d), cGAS (e, f), IFI16 (g, h) and IRF3 (i, j). mRNA fold change of gene targets of mtDNA release, *ifna1* (k), *ifna4* (l), and *ifnb* (m), was measured by qPCR. All the protein bands were normalized over β -actin (37 kD) and percentage intensity relative to control was analyzed. Data was analyzed using one-way ANOVA with Tukey's multiple comparison test

(* $p < 0.05$, ** $p < 0.01$, *** $p < 0.001$, **** $p < 0.0001$) and represented as mean \pm SEM with $n = 3/\text{treatment}$ (* indicates significant difference from control).

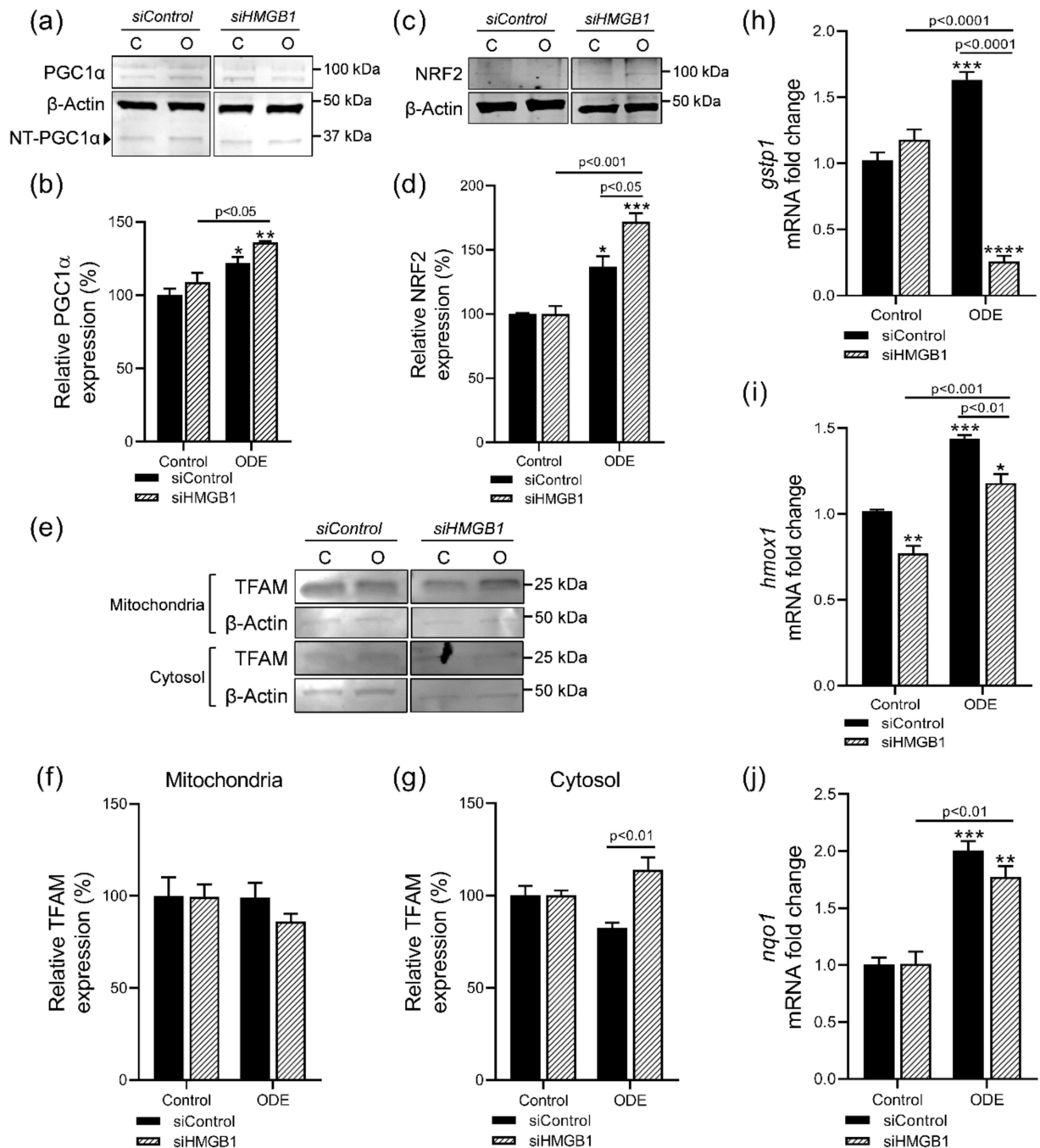


Fig. 5. Lack of HMGB1 promotes mitochondrial biogenesis in OD exposed NHBE cells. Markers of mitochondrial biogenesis in NHBE cells with or without siRNA mediated HMGB1 knockdown and treated with OD (1%) for 24 h was measured. Immunoblotting of whole cell lysates of NHBE cells was performed to measure PGC1α (a, b) and NRF2 expression (c, d). TFAM expression was compared in the mitochondrial (e, f) and cytosolic (e, g) fractions of the NHBE cells. mRNA fold change of gene targets downstream of NRF2, *gstp1* (h), *hmox1* (i), and *nqo1* (j), was measured by qPCR. All the protein bands were normalized over β-actin (37 kDa) and percentage intensity relative to control was analyzed.

Data was analyzed using one-way ANOVA with Tukey's multiple comparison test (* $p < 0.05$, ** $p < 0.01$, *** $p < 0.001$, **** $p < 0.0001$) and represented as mean \pm SEM with $n = 3$ /treatment (* indicates significant difference from control).

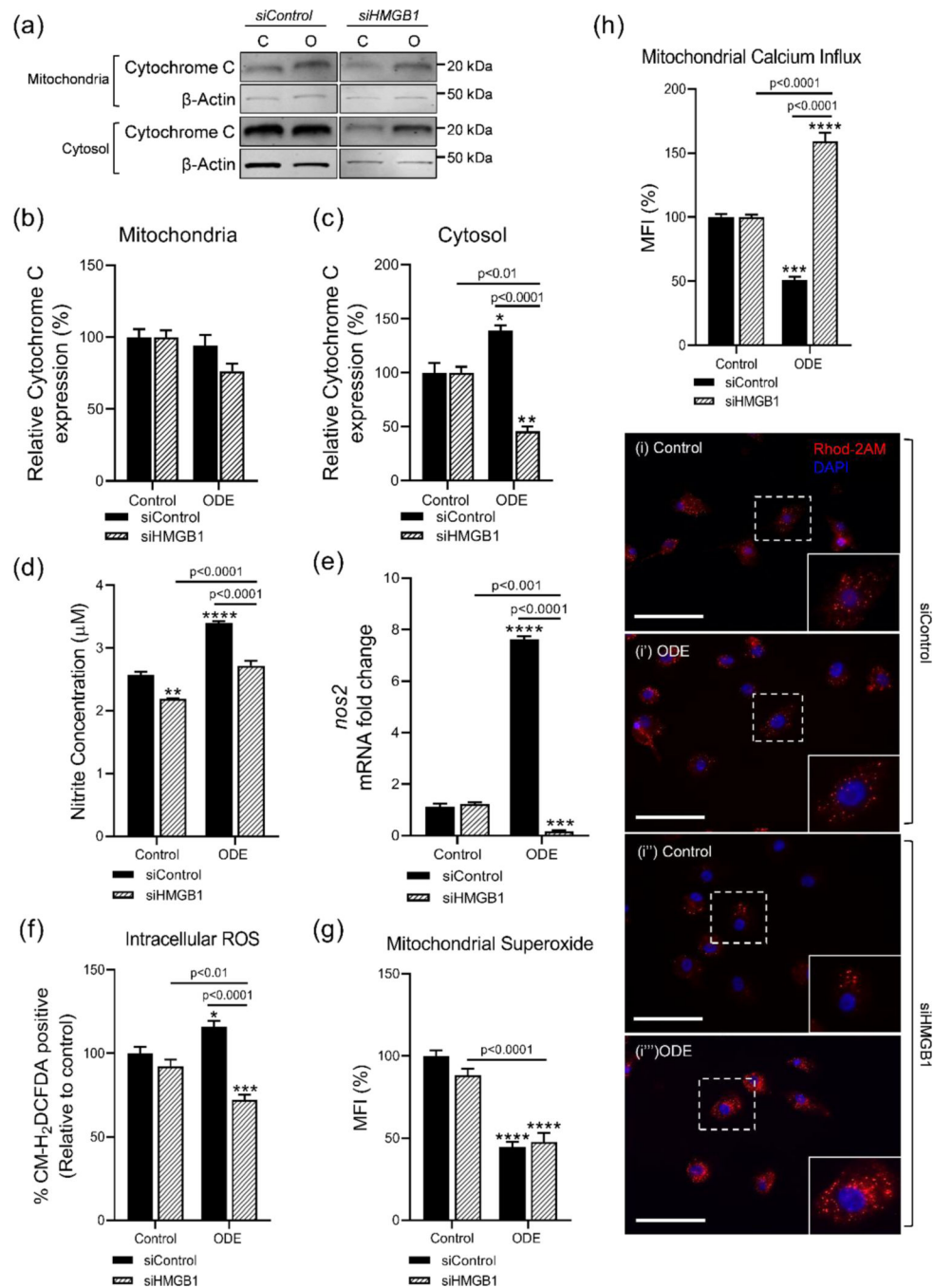


Fig. 6. Acute OD exposure causes cytochrome c release into the cytosol.

Immunoblotting of mitochondrial and mitochondria-free cytosolic fractions of NHBE cells with or without siRNA mediated HMGB1 knockdown and treated with ODE (1%) for 24 h, to detect the presence of Cytochrome C. Cytochrome C expression was compared between the mitochondrial (a, b) and cytosolic (a, c) fractions of the cells. Concentration of secreted nitrites was measured using griess assay (d) and mRNA levels of *nos2* (e) was measured by qPCR. Using CM-H₂DCFDA and Mito-SOX dyes, the levels of superoxide anions (SOX) intracellularly (f) and within the mitochondria (g) was measured, respectively. Intra-

mitochondrial calcium levels in mitochondria isolated from the treated cells was quantified (h) and visualized (i-i''''; Scale bar = 100 μ m) by Rhod-2AM staining. For western blot, all the protein bands were normalized over β -actin (37 kD) and percentage intensity relative to control analyzed. Data was analyzed using one-way ANOVA with Tukey's multiple comparison test (* $p < 0.05$, ** $p < 0.01$, *** $p < 0.001$, **** $p < 0.0001$) and represented as mean \pm SEM with $n = 3-6$ /treatment (* indicates significant difference from control).

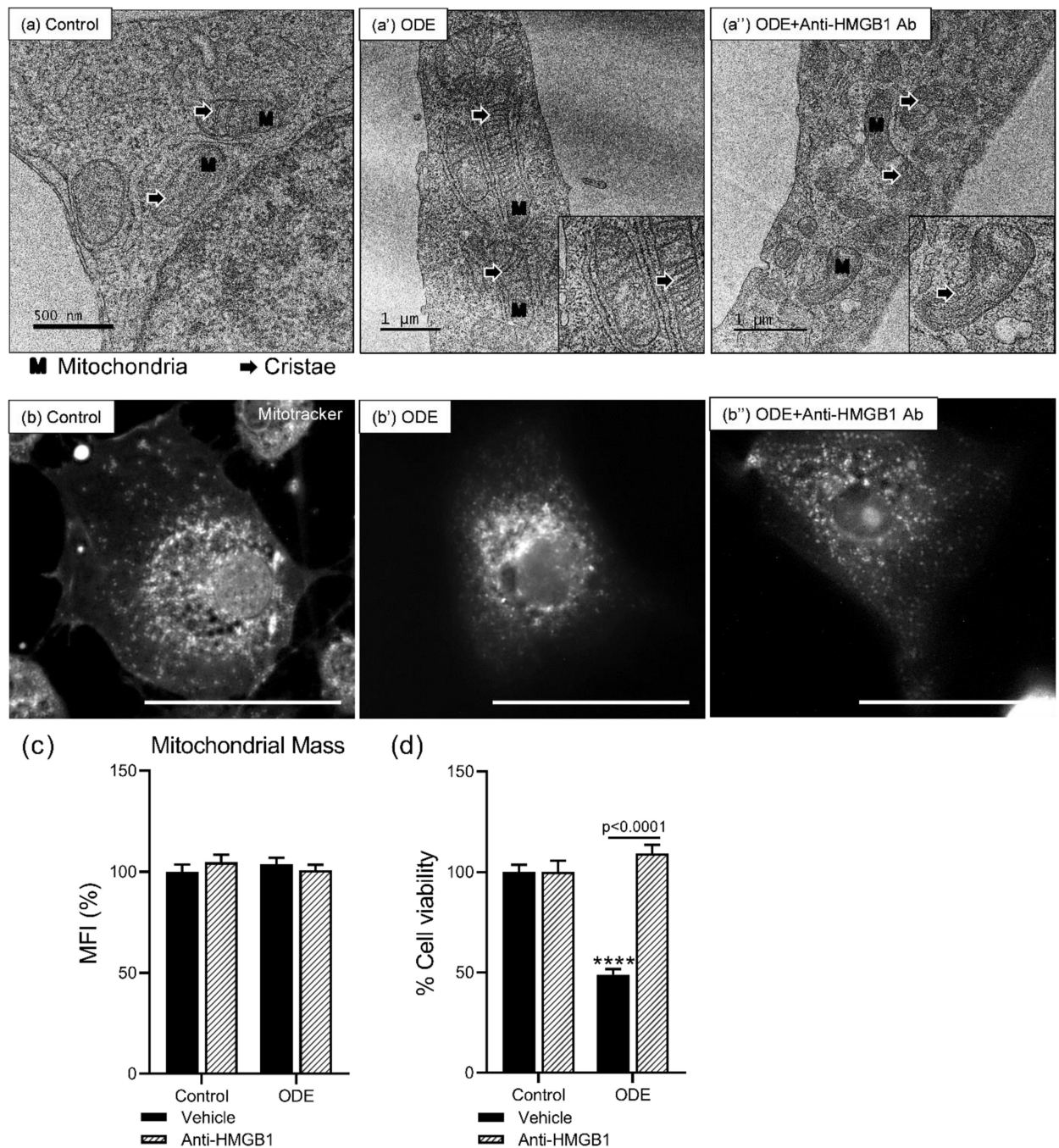


Fig. 7. Antibody mediated neutralization of HMGB1 maintains mitochondrial morphology and cell viability.

Transmission electron microscopy (TEM) of NHBE cells treated with medium or ODE (1%) followed by medium or HMGB1 neutralization antibody (10 µg/mL) for 8 h per day for 5 days show changes in the mitochondrial morphology. A number of mitochondria displayed fused and elongated mitochondrial morphology (a-a''); scale bar, 0.5–1 µm) on treatment with ODE. Cells treated with ODE followed by HMGB1 neutralization showed noticeably healthier mitochondria with a few morphological changes. Mitochondrial mass was measured (c) and the morphology was visualized by staining with Mito-tracker dye (b-

b''; Scale bar = 100 μ m). MTT assay was performed to measure cell viability on treatment (d). Data was analyzed using one-way ANOVA with Tukey's multiple comparison test (* $p < 0.05$, ** $p < 0.01$, *** $p < 0.001$, **** $p < 0.0001$) and represented as mean \pm SEM with $n = 6$ /treatment (* indicates significant difference from control).

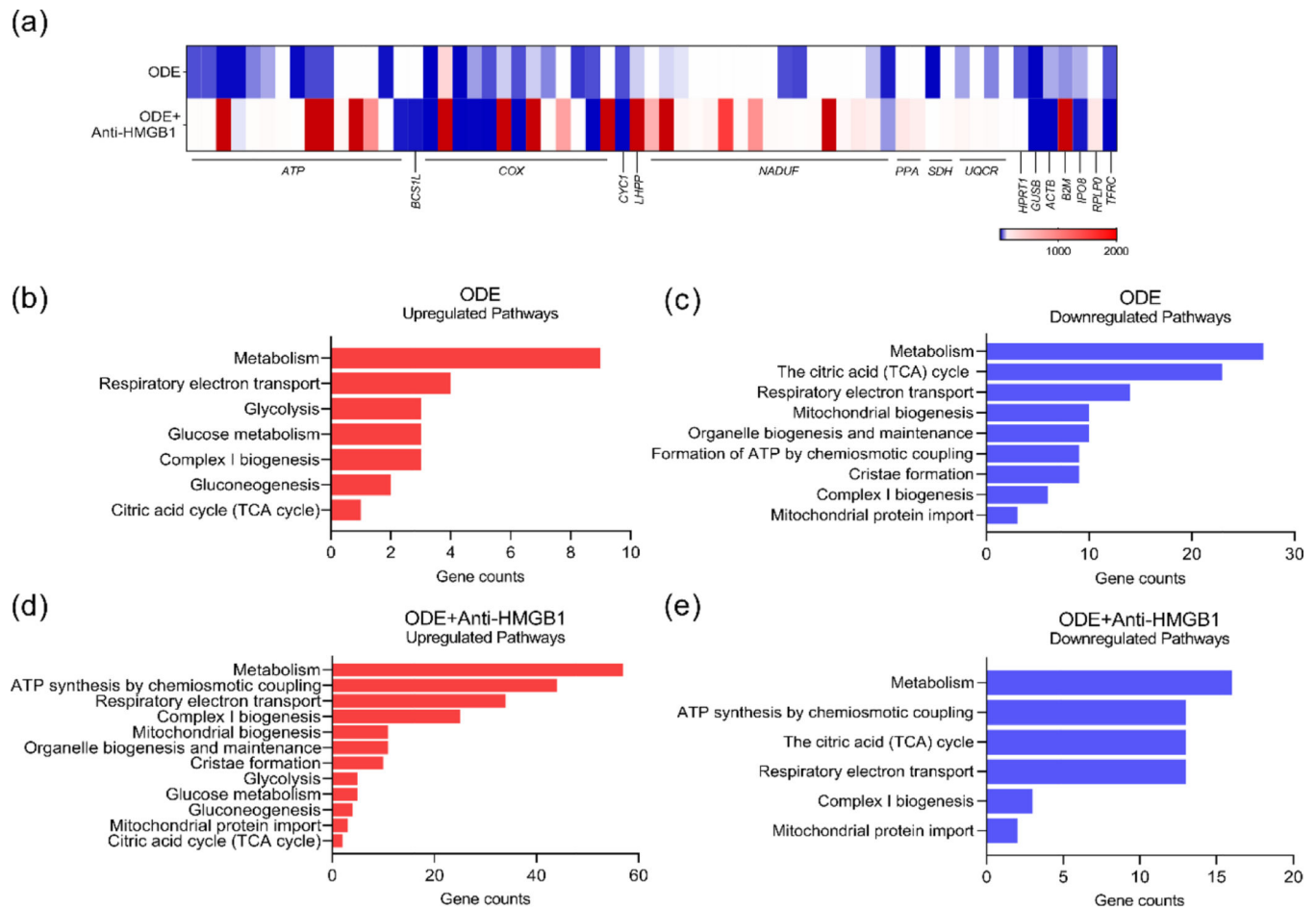


Fig. 8. HMGB1 neutralization upregulates genes associated with mitochondrial respiration. mRNA expression profiles of genes specific to mitochondrial respiration in NHBE cells treated with medium or ODE (1%) followed by medium or HMGB1 neutralization antibody (10 $\mu\text{g/mL}$) for 8 h per day for 5 days was measured using a targeted gene array. Heatmap of mRNA transcripts of genes that had a 10-fold change in expression were selected (a). Selected upregulated (b, d) and downregulated (c, e) pathways from reactome pathway analysis of significantly altered mRNA transcripts with FDR corrected p-value cut-off <0.05 were selected and represented by gene counts. Data was analyzed using one-way ANOVA with Tukey's multiple comparison test (* $p < 0.05$, ** $p < 0.01$, *** $p < 0.001$, **** $p < 0.0001$) and represented as mean \pm SEM with $n = 2/\text{treatment}$ (* indicates significant difference from control).

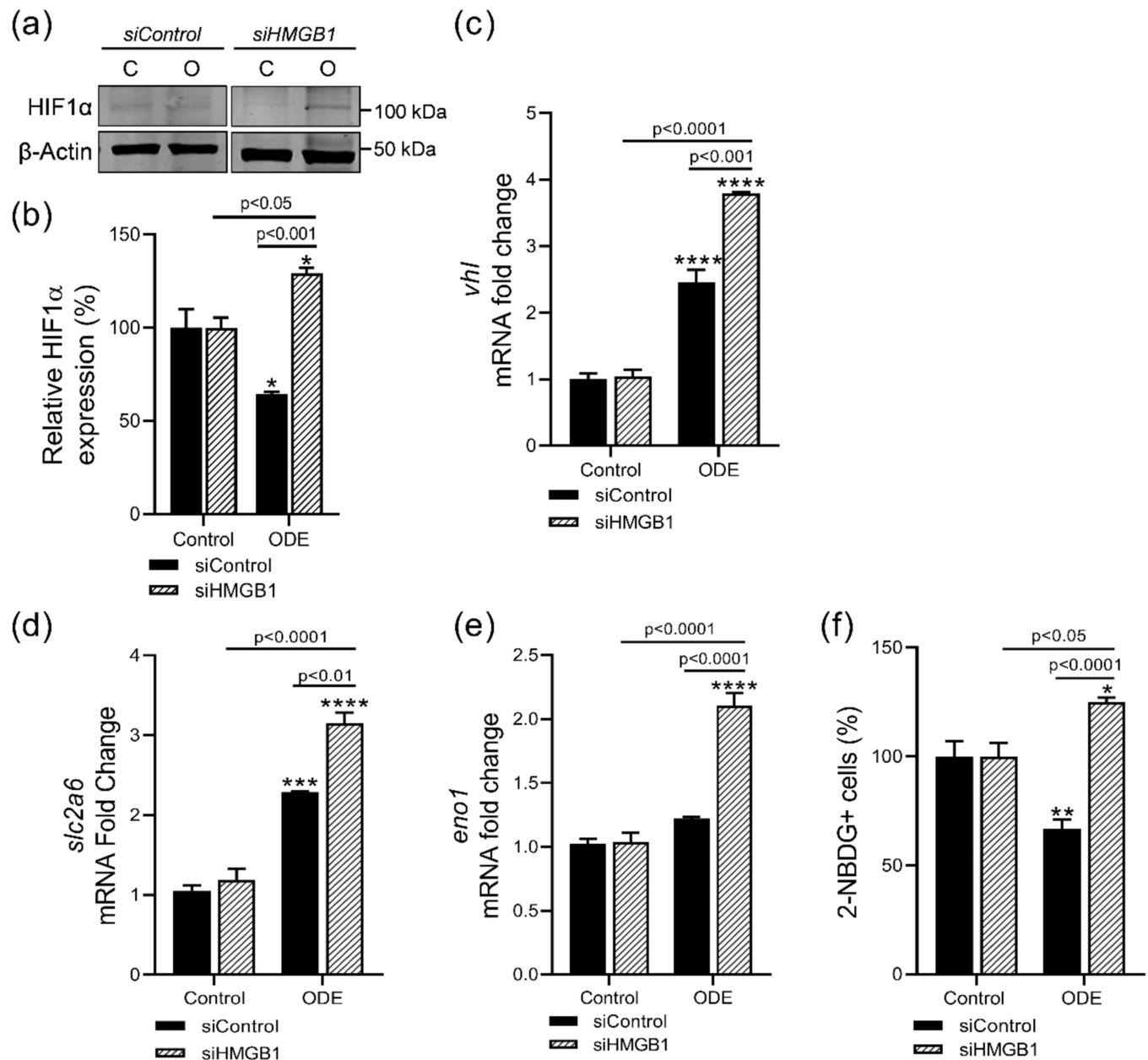


Fig. 9. Lack of HMGB1 initiates hypoxia response on acute OD exposure.

Markers of hypoxia response in NHBE cells with or without siRNA mediated HMGB1 knockdown and treated with ODE (1%) for 24 h was measured. Immunoblotting of whole-cell lysates of NHBE cells were performed to measure HIF1α (a, b). mRNA fold change of ubiquitin ligase, *vhl* (c), and *slc2a6* (d) and *eno1* (e), involved in glucose uptake and glycolysis, were measured by qPCR. 2-NBDG uptake to measure cellular glucose uptake was performed (f). For western blot, all the protein bands were normalized over β-actin (37 kD) and percentage intensity relative to control analyzed. Data was analyzed using one-way ANOVA with Tukey's multiple comparison test (*p < 0.05, **p < 0.01, ***p < 0.001, ****p < 0.0001) and represented as mean ± SEM with n = 3–6/treatment (* indicates significant difference from control).

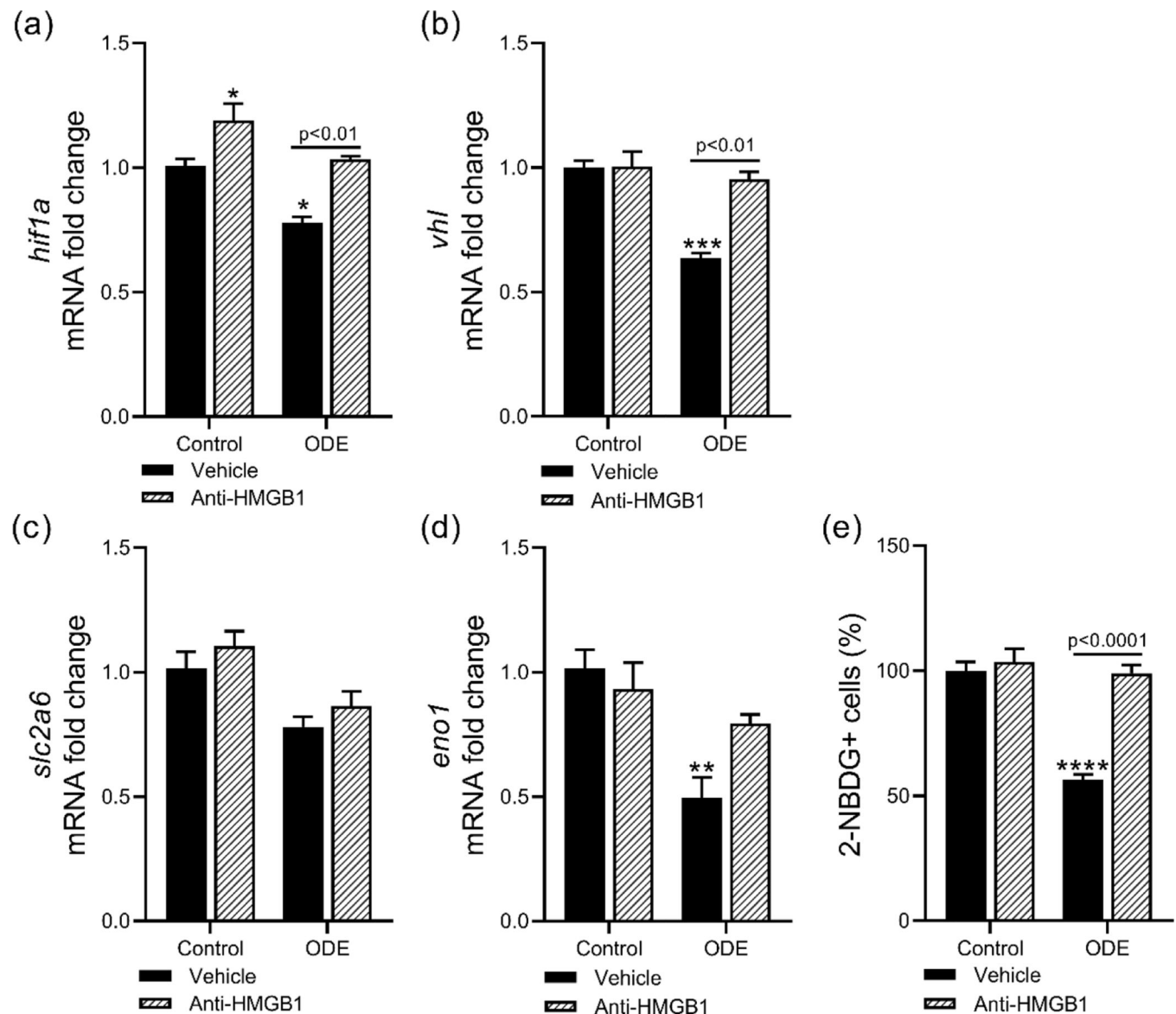


Fig. 10. Normoxic conditions are maintained on HMGB1 neutralization during chronic OD exposure.

Markers of hypoxia response in NHBE cells treated with medium or ODE (1%) followed by medium or HMGB1 neutralization antibody (10 μ g/mL) for 8 h per day for 5 days was measured. mRNA fold change of hypoxia response factor, *hif1a* (a) and ubiquitin ligase, *vhl* (b), and *Slc2a6* (c) and *Eno1* (d), involved in glucose uptake and glycolysis were measured by qPCR. 2-NBDG uptake to measure cellular glucose uptake was performed (e). Samples for all assays were derived from the same experiment and were processed in parallel. Data was analyzed using one-way ANOVA with Tukey's multiple comparison test (*p < 0.05, **p < 0.01, ***p < 0.001, ****p < 0.0001) and represented as mean \pm SEM with n = 3–6/treatment (* indicates significant difference from control).

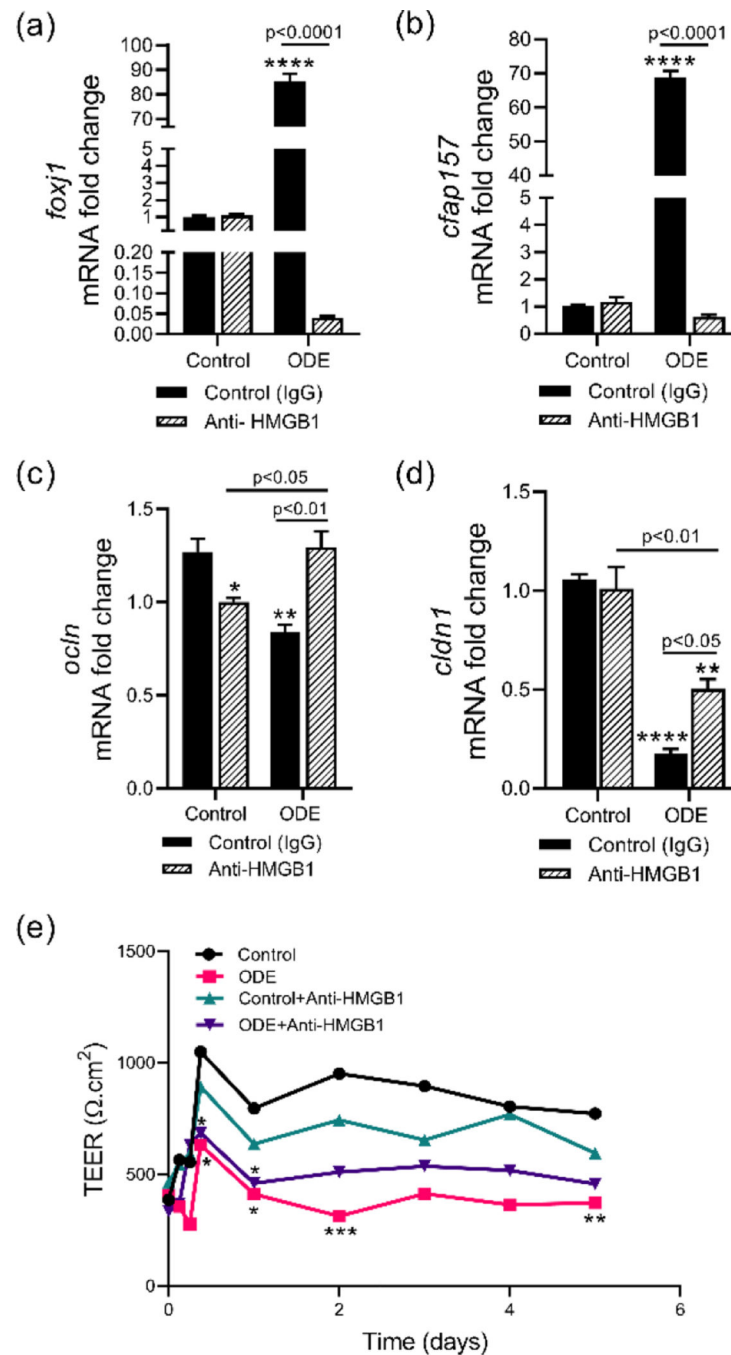


Fig. 11. HMGB1 neutralization upregulates tight junction integrity in ALL.

NHBE cells differentiated on air-liquid interface (ALI) culture treated with medium or ODE (1%) followed by medium or HMGB1 neutralization antibody (10 $\mu\text{g/mL}$) for 1 h per day for 5 days. mRNA fold change of markers of motile cilia, *foxj1* (a) and *cfap157* (b), and tight junction, *ocln* (c) and *cldn1* (d), was measured by qPCR. Tight junction integrity was assessed by trans-epithelial electrical resistance (TEER) measurement (e). Samples for all assays were derived from the same experiment and were processed in parallel. Data was analyzed using one-way ANOVA with Tukey's multiple comparison test (*p < 0.05, **p <

0.01, *** $p < 0.001$, **** $p < 0.0001$) and represented as mean \pm SEM with $n = 3$ /treatment (* indicates significant difference from control).

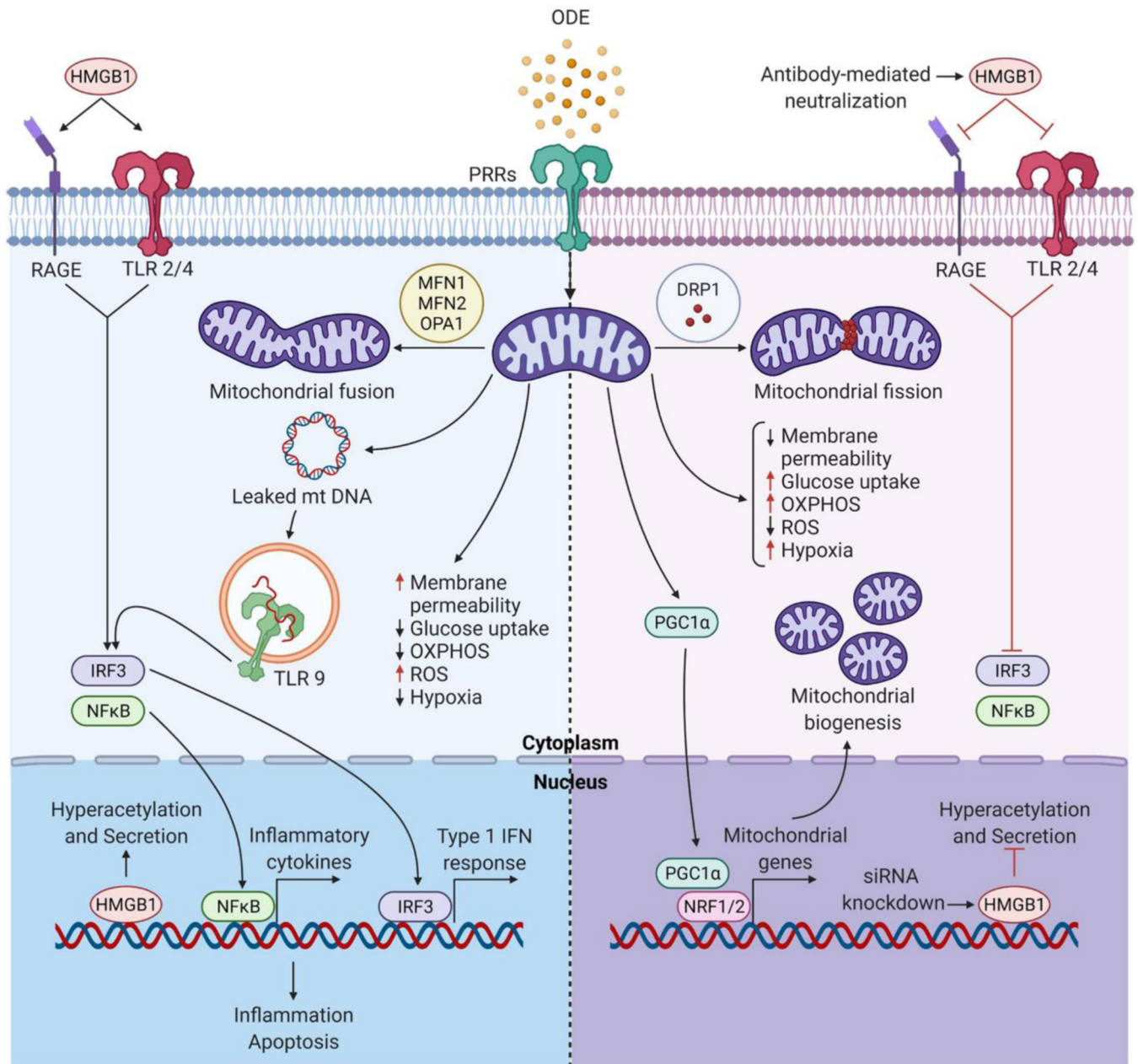


Fig. 12. An overview of impact of HMGB1 on ODE exposure induced mitochondrial dysfunction in NHBE cells.

HMGB1 increases autophagy, inhibits apoptosis, and regulates mitochondria functions. ODE exposure promoted mitochondrial fusion and mtDNA release promoting a pro-inflammatory response through TLR9, NF κ B, and IRF3 signaling pathways resulting in pro-inflammatory cytokine release. On the other hand, HMGB1 knockdown or use of Anti-HMGB1 antibody rescues ODE-induced mtDNA release and promotes mitochondrial fission. ODE exposure also induces a decrease in OXPHOS and glucose uptake while increasing ROS generation and mitochondrial membrane permeability. HMGB1 knockdown or use of Anti-HMGB1

antibody treatment decreases ROS generation, promotes mitochondrial biogenesis, and upregulates markers associated with OXPHOS.

Author Manuscript

Author Manuscript

Author Manuscript

Author Manuscript

Table 1.

Endotoxin concentrations in ODE

Sample No.	Endotoxin (EU/mL)
1	1.140 ± 0.001
2	0.990 ± 0.0005
3	1.337 ± 0.0006
4	1.433 ± 0.02
5	1.417 ± 0.002
6	0.8067 ± 0.0008
7	1.263 ± 0.7

Table 2.

Stock and working concentrations of treatments

Treatment	Stock concentration	Working concentration (in BEGM/DPBS)
ODE	100% in HBSS	1%
Anti-HMGB1 neutralization Antibody	1.8 mg/mL	10 µg/mL

Author Manuscript

Author Manuscript

Author Manuscript

Author Manuscript